

USS 10/Library

SIT-P251 (6/70)

N71-19208

NASA CR-116871

UNCLASSIFIED

DEPARTMENT OF PHYSICS

CASE FILE COPY

Proximity Effect Between Superconducting and
Normal Metals

First Technical Report

Josephson Tunneling Through Normal Metal Barriers

June 1970

Hans Meissner

and

Roger R. Rockefeller

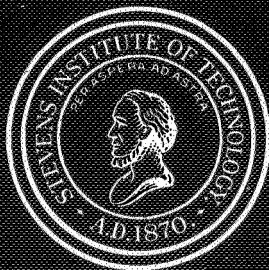
NASA Grant No. NGL 31-003-020

Office of Research Grants and Contracts

Office of Space Science and Applications

National Aeronautics and Space Administration

Washington, D. C. 20546



STEVENS INSTITUTE
OF TECHNOLOGY

CASTLE POINT STATION
HOBOKEN, NEW JERSEY 07030

JOSEPHSON TUNNELING
THROUGH NORMAL METAL BARRIERS

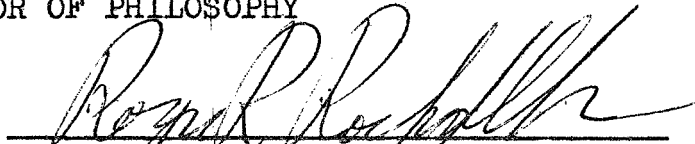
by

Roger R. Rockefeller

A DISSERTATION

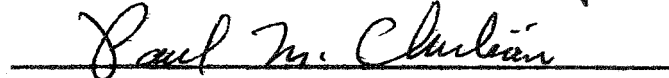
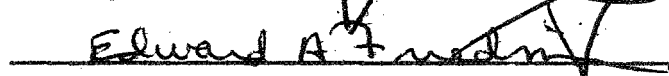
Submitted to the Faculty of the Stevens Institute of
Technology in partial fulfillment of the requirements
for the degree of

DOCTOR OF PHILOSOPHY



Roger R. Rockefeller, Candidate

SUPERVISORY COMMITTEE

 Chairman

STEVENS INSTITUTE OF TECHNOLOGY
Castle Point, Hoboken, New Jersey

1970

UNCLASSIFIED

Stevens Institute of Technology

Department of Physics

Castle Point Station

Hoboken, New Jersey 07030

Proximity Effect Between Superconducting and

Normal Metals

First Technical Report

Josephson Tunneling Through Normal Metal Barriers

June 1970

Hans Meissner

and

Roger R. Rockefeller

NASA Grant No. NGL 31-003-020

Office of Research Grants and Contracts

Office of Space Science and Applications

National Aeronautics and Space Administration

Washington, D. C. 20546

Josephson Tunneling
Through Normal Metal Barriers

ABSTRACT

New phase-lock techniques have been employed to study the electrical and magnetic properties of superconductor-normal metal-superconductor junctions. The junctions were of the mechanical contact type, using tin and gold.

Josephson tunneling was observed through $10,500\text{\AA}^0$ of gold, and the current-voltage characteristics were found to agree with current theories, including the effects of fluctuations.

Voltage-magnetic field characteristics were used to verify the existence of "excess supercurrents" in the junction, and to determine the previously unknown current carrying area of the junction.

A model, based on the deGennes theory and taking into account the effect of barrier resistance, was proposed to explain the data. The critical current

dependence on the normal metal thickness, resistance and temperature was in agreement with the theory.

It was found experimentally that the I-V characteristics can be modified by a control current, introduced directly into the N region of the SNS junction.

Author: Roger R. Rockefeller

Advisor: Professor Hans Meissner

May, 1970

TABLE OF CONTENTS

I.	INTRODUCTION	
A.	History and Background	1
B.	Theoretical Background	2
C.	Non-Local Electrodynamics	8
D.	The Microscopic Theory	10
E.	The Ginzburg-Landau Theory	11
II.	THEORY Of The EXPERIMENT	
A.	The Ginzburg-Landau Theory Applied to N-S Junctions	17
B.	The deGennes Theory of an N-S Junction	19
C.	The Josephson Effect	24
D.	Magnetic Properties of the Josephson Junction	31
E.	Electrical Characteristics of the Josephson Junction	37
III.	DESCRIPTION Of The EXPERIMENT	
A.	Introduction	48
B.	The Cryostat	50
C.	The Sample Holder	52
D.	Sample Preparation	56
E.	Magnetic Field Coils	60
F.	Measurements	61

IV. EXPERIMENTAL RESULTS

A. The Contact Area	70
B. The Critical Current Density	74
C. Transition Curves	96
D. Current-Voltage Characteristics of the Contact	100
E. The Voltage-Magnetic Field Characteristics	103
F. The Modification of the I-V Characteristics With a Control Current	110

V. CONCLUSIONS	112
----------------	-----

BIBLIOGRAPHY

ACKNOWLEDGEMENTS

I. Introduction.

I.A. History and Background.

The discovery of superconductivity became possible when Kamerlingh Onnes succeeded in liquifying helium. Liquid helium exists at a temperature of 4.2 degrees Kelvin (K) under atmospheric pressure and it provides one with a liquid bath environment for the study of phenomena at low temperatures.

While studying the properties of mercury at low temperatures, Onnes noticed^{1,2} that the electrical resistance of his sample became immeasurably small below 4K. This was the discovery of superconductivity. Soon, there were many polyvalent metals found whose resistance apparently dropped to zero below a characteristic temperature called the transition temperature, T_c . The metals that exhibit this behavior are called superconductors and the currents that flow through them, in the absence of a

1. H. Kamerlingh Onnes, Leiden Comm., 122b, 124c (1911).

2. H. Kamerlingh Onnes, Leiden Comm., Suppl. No. 34 (1913).

resistance, are called supercurrents. It was also noticed that, in an applied magnetic field H , the superconductor loses its property of zero resistance. The characteristic field for which this occurs is called the critical field H_c .

In 1933, Walther Meissner and R. Ochsenfeld showed that a superconductor is not accurately described as just an ideal conductor.³ In addition to its property of zero resistance, it acts like a perfect diamagnetic material. The discovery that a superconductor will expel magnetic flux, B , from its interior implies that the transition from the superconducting state to the non-superconducting (normal) state is thermodynamically reversible. It follows that $H = -4\pi M$ inside the superconductor in an applied field, where M is the magnetization.

I.B. Theoretical Background.

Thermodynamics was first applied to the problem of

3. W. Meissner and R. Ochsenfeld, Naturwiss 21, 787 (1933).

superconductivity by Gorter and Casimir⁴. In a magnetic field, the Gibbs free energy is given by,

$$G_s(T, H) = G_s(T, 0) + H^2/8\pi \quad \text{I.B.1}$$

which leads to the free energy difference between the normal and superconducting states,

$$G_n(T, 0) - G_s(T, 0) = H_c^2/8\pi. \quad \text{I.B.2}$$

The basic thermodynamic approach to superconductivity is to find an expression for the free energy of the particular superconducting state being examined. Then, this expression is minimized, using the calculus of variations. This procedure yields conditions for the equilibrium state of the system. An example of this approach will give one the spatial dependence of H in a superconductor. The free energy is written in terms of the magnetic field,

4. C. Gorter and H.B.G. Casimir, *Physica* 1, 306 (1934).

5. P.G. deGennes, Superconductivity of Metals and Alloys (W.A. Benjamin, Inc., New York, 1966), Chapter 1.

$$G_s(H) = E_0 + E_{kin}(H) + E_{mag}(H) \quad \text{I.B.3}$$

where E_0 is the total free energy of the electrons at rest in the superconductor, E_{kin} is the kinetic energy of the superconducting currents and E_{mag} is the energy associated with the applied magnetic field. This equation becomes,

$$G_s(H) = E_0 + (1/8\pi) \int (H^2 + \lambda_L^2 |\nabla \times \underline{H}|^2) d^3r \quad \text{I.B.4}$$

with λ_L equal to,

$$\lambda_L = (mc^2/4\pi n_s e^2)^{\frac{1}{2}} \quad \text{I.B.5}$$

and m is the effective mass of the electron, c is the velocity of light, e is the charge of the electron, and n_s is the density of superconducting electrons in the metal*. Here, n_s refers to the Gorter and Casimir⁴

* CGS units will be used throughout this work unless otherwise noted.

phenomenological two-fluid model of superconductivity^{*}. Assuming that n_s is independent of H and using the calculus of variations, a condition on H is found. In the case of a semi-infinite, flat, superconducting slab the tangential magnetic field is given by,

$$H_x(z) = H_x(0) \exp(-z/\lambda_L) \quad \text{I.B.6}$$

in the superconductor. The normal to the surface is in the z -direction. That is, the magnetic field penetrates the superconductor for a distance on the order of λ_L , called the London penetration depth, after the men^{6,7} who proposed it. Typically, λ_L is of the order of 10^{-5} to 10^{-6} cm.

^{*}Here, it is assumed that in the superconducting phase, a certain fraction of the conduction electrons condense into an ordered state which does not contribute to the entropy of the system. These are the so-called superconducting electrons. The remaining electrons are in the normal state. While not rigorously correct in the light of the current microscopic theory, this model is useful in picturing many aspects of superconductivity.

6. F. London and H. London, Proc. Roy. Soc. A149, 71(1935).

7. F. London and H. London, Physica, 2, 341 (1935).

The Meissner effect and Eq. I.B.6 can also be derived from electrodynamic equations if one replaces Ohm's law by another relationship in a superconductor. The supercurrent density, \underline{j}_s , is written as,

$$\underline{j}_s(r) = -(c/4\pi\lambda_L^2)\underline{A} \quad \text{I.B.7}$$

where \underline{A} is the vector potential defined by $\nabla \times \underline{A} = \underline{H}$ in the gauge $\nabla \cdot \underline{A} = 0$. The force equation, $m \, dy/dt = -e\underline{E}$ may be written (using the relation, $\underline{j}_s = -n_s e \underline{v}$) as,

$$d\underline{j}_s/dt = (c^2/4\pi\lambda_L^2)\underline{E} \quad \text{I.B.8}$$

Equations I.B.7 & I.B.8 are known as the London^{6,7} equations. They can be combined to give Eq. I.B.6 as well as other features of superconductivity and are especially important in that they show the relationship between the supercurrent and the magnetic field.

In the absence of a magnetic field, the superconductor experiences a transition of the second order in going to the normal state. In a magnetic field, the transition occurs when $T < T_c(H = 0)$ and it is a first order transition. The critical field is temperature dependent and is

described to within a few percent by,

$$H_c(T) = H_c(0)[1 - (T/T_c)^2] \quad \text{I.B.7}$$

This is plotted in Fig. 1. This figure is also an

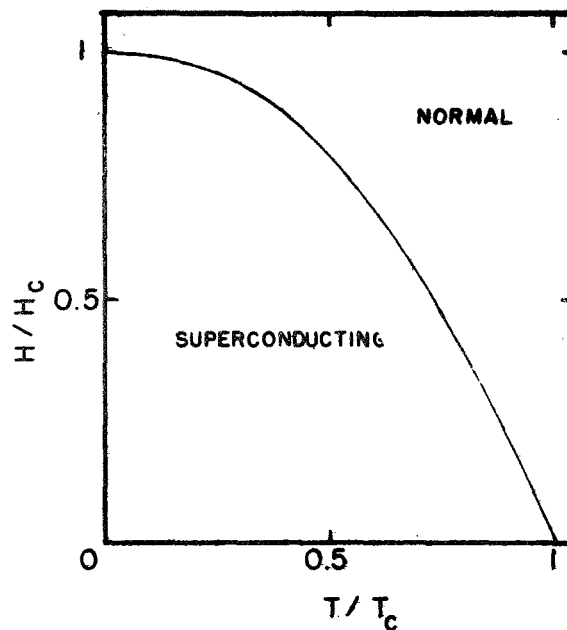


Fig. 1. The Critical
Magnetic Field vs Temperature.

equilibrium phase diagram. The state of the system, at any point on the diagram, is independent of the path that is taken to reach it.

I.C. Non-Local Electrodynamics.

From experiments, Pippard^{8,9} realized that the penetration depth was a function of the mean-free-path, ℓ . This fact becomes apparent when λ_L is of the order of ℓ . Following a similiar treatment used in the anomalous skin effect in normal metals, Pippard proposed that the local London equation (Eq. I.B.7) be replaced by the non-local relation,

$$\vec{j}_S(0) = (3c/16\pi^2 \xi_0 \lambda_L^2) \int \frac{\vec{r}(\vec{r} \cdot \vec{A})}{r^4} \exp(-r/\xi) d^3r \quad \text{I.C.1}$$

Here, ξ_0 is a constant, while $\xi = \xi(\ell)$. Both have the units of length. ξ_0 is an intrinsic length (called the intrinsic coherence length) of the pure superconductor at $T = 0$. $\xi(\ell)$ is a characteristic length of the superconductor which describes the distance over which the effects of a perturbing force are important. It is called the Pippard coherence length. The functional dependence of $\xi(\ell)$ was not theoretically determined and experiment-

8. A.B.Pippard, Proc.Roy.Soc. (London) A203, 210 (1950).

9. A.B.Pippard, Proc.Roy.Soc. (London) A216, 547 (1953).

ally it obeyed a relation,

$$1/\xi(l) = 1/\xi_0 + 1/0.8l \quad \text{I.C.2}$$

This indicates that $\xi(l)$ is always smaller than ξ_0 and approaches ξ_0 as $l \rightarrow \infty$. ξ_0 can be determined from the microscopic theory (and was experimentally determined by Pippard) and is,

$$\xi_0 = 0.18 \hbar v_f / kT_c \quad \text{I.C.3}$$

v_f is the Fermi velocity. ξ_0 is approximately the minimum size of an ensemble of electrons, at the Fermi surface, with an energy kT_c .

To summarize, Pippard had shown that the superconducting electrons (or their quantum mechanical wave functions) are not rigid in an applied magnetic field, but could be perturbed, from a point, over a distance $\xi(l)$. That is, the coherence length is the minimum distance over which any substantial change in the properties of a superconductor can take place.

I.D. The Microscopic Theory.

The microscopic theory is a quantum mechanical theory that describes superconductivity within the framework of electrons interacting in a metal lattice. The groundwork was done by H. Frölich¹⁰ who noted that electrons, in a lattice, may experience attractive interactions through coupling by lattice vibrations (phonon coupling). He was able to show that some phenomena such as the isotope effect followed from these interactions.

In 1956, Cooper¹¹ was able to show that a pair of electrons, just above the Fermi surface, could form a bound state if there were any sort of attractive force between them. This led to the fundamental Bardeen, Cooper, Schrieffer¹² (BCS) theory.

BCS envision a ground state of the electronic system composed of Cooper (electron) pairs. These are electrons with equal and opposite spin and momentum, coupled by

10. H. Frölich, Phys. Rev. 79, 845 (1950).

11. L.N. Cooper, Phys. Rev. 104, 1189 (1956).

12. J. Bardeen, L.N. Cooper and J.R. Schrieffer, Phys. Rev. 106, 162 (1957); 108, 1175 (1957).

phonon interactions and separated by as much as a coherence length. The ground state is separated from the excited states by an energy gap $\Delta(T)$ which is essentially the energy required to break up a Cooper pair. The BCS theory characterizes a metal by its Debye temperature, Θ , its electron density of states at the Fermi level, $N(E_F)$, and an electron-lattice-electron interaction potential, V . It predicts a transition temperature,

$$T_c = 1.14 \Theta \exp[-1/N(E_F)V] \quad \text{I.D.1}$$

which is adequately confirmed by experiment. The BCS theory also confirms the existence of Pippard's intrinsic coherence length (Eq. I.C.3) and supplies the value of the constant 0.18 .

I.E. The Ginzburg-Landau Theory.

In 1950 , well before the development of the microscopic theory, Ginzburg and Landau¹³ produced a powerful and intuitively satisfying phenomenological theory of

13. V.I. Ginzburg and L.D. Landau, J.E.T.P. 20, 1064 (1950).

superconductivity. They proposed the existence of a complex function, $\psi(r)$, to characterize the superconducting state of a material. They assumed that $\psi(r)$ represented some "effective wave function" of the superconducting electrons. They chose a normalization such that $\psi^*(r) \psi(r)$ represented the density of superconducting electrons. Ginzburg and Landau (GL) point out that $\psi(r)$ is only determined to within a multiplicative phase factor of $\exp(i\theta)$, since all observable quantities involve the product $\psi^* \psi$. They then choose a free energy approach to find relations for ψ and other variables of the problem. The following analysis is a synthesis of the work of de-Gennes⁵, Mercereau¹⁴, Chandrasekhar¹⁴, Werthamer¹⁴, Josephson¹⁴, and Lynton¹⁵.

The free energy of a superconductor can be expanded in terms of its characteristic parameter $\psi^* \psi = |\psi|^2$. The term ψ will be referred to as the "order parameter". Near the transition temperature, $|\psi|^2$ is small and an expression to the second order in $|\psi|^2$ is valid. That is,

14. Superconductivity (Marcel Dekker, Inc., New York, 1969) edited by R.D. Parks. Chapters 8, 1, 6 & 9.
15. E.A. Lynton, Superconductivity (John Wiley & Sons, New York, 1964).

$$G(|\psi|^2) = G_N + \alpha |\psi|^2 + \frac{\beta}{2} |\psi|^4 \quad \text{I.E.1}$$

in the absense of a magnetic field. The quantities α and β are expansion coefficients to be determined. If we include the effect of a magnetic field, two terms must be added to Eq. I.E.1. The first is,

$$(1/2m)[(-i\hbar\nabla - 2e\mathbf{A}/c)\psi]^2 \quad \text{I.E.2}$$

which preserves the gauge invariance of G in a magnetic field. It is noteworthy that the term $\nabla\psi$ is that term which leads to an energy associated with a spatial variation of ψ (due to the presence of \mathbf{A} , for instance). This is equivalent to saying that ψ cannot change too quickly with distance (it requires too much energy) and thus introduces the concept of a range of coherence. The second term to be added is the energy $H^2/8\pi$.

The coefficients α and β can be shown (Ref.5, page 175) to be,

$$\alpha(T) = (T_c - T) \left. \frac{\partial \alpha}{\partial T} \right|_{T=T_c} \cong (\hbar^2/m\xi_0^2)(T - T_c)/T \quad \text{I.E.3}$$

$$\beta(T) = \beta(T_c) \cong (1/N)(\hbar/m\xi_0^2 kT_c)^2 \quad \text{I.E.4}$$

near T_c . Note that α is temperature dependent.

Minimizing the free energy expression with respect to ψ and \underline{A} , the following equations for equilibrium are obtained.

$$\alpha\psi + \beta|\psi|^2\psi + (1/2m)(-i\hbar\nabla - 2e\underline{A}/c)^2\psi = 0 \quad \text{I.E.5}$$

$$(-c\nabla^2\underline{A}/4\pi) = \underline{j}_s = (e\hbar/im)(\psi^*\nabla\psi - \psi\nabla\psi^*) - (4e^2/mc)\psi^*\psi\underline{A} \quad \text{I.E.6}$$

These are the Ginzburg-Landau equations. The boundary conditions to be used with these equations are,

$$(-i\hbar\nabla - 2e\underline{A}/c)_n\psi = 0 \quad \text{I.E.7}$$

for the vacuum-superconductor interface, and,

$$(-i\hbar\nabla - 2e\mathbf{A}/c)_n\psi = ia_0\psi \quad \text{I.E.8}$$

for the interface between a normal metal and a superconductor. a_0 is a real constant.

For weak fields, where ψ does not change spatially, that is when $\nabla\psi \sim 0$, the GL equation I.E.6 reduces to London's equation, or its equivalent form,

$$\nabla_{\mathbf{A}}^2 \cong (16\pi e^2/mc^2)|\psi|_{\mathbf{A}}^2 = 4\lambda_{\mathbf{A}}^2 \quad \text{I.E.9}$$

where the factor of 4 comes from the fact that a Cooper pair has a charge of $-2e$, and $n_s = |\psi|^2$ has been used.

To illustrate how a characteristic coherence length follows from the GL equations, consider the case where $\psi = \psi(x)$ and the currents and magnetic fields are small. Eq. I.E.5 reduces to,

$$-(\hbar^2/2m)d^2\psi/dx^2 + \alpha\psi + \beta\psi^3 = 0 \quad \text{I.E.10}$$

where, in an unperturbed superconducting state, $\psi(x)$ is just the constant given by,

$$\psi^2(x) = \psi_0^2 = -\alpha/\beta \quad \text{I.E. 11}$$

Now consider what happens when the superconductor undergoes a change at some point, so that $\psi(x)$ is perturbed. Eq. I.E. 10 can be simplified by writing it in terms of a reduced order parameter, $\Psi(x)$, such that,

$$\Psi(x) = \psi(x)/\psi_0 = (-\beta/\alpha)^{1/2} \psi(x) \quad \text{I.E. 12}$$

Then Eq. I.E. 10 reduces to¹⁶

$$\xi_{GL}^2 d^2 \Psi / dx^2 + \Psi - \Psi^3 = 0 \quad \text{I.E. 13}$$

with,

$$\xi_{GL}^2 = \hbar^2 / 2m|\alpha| \quad \text{I.E. 14}$$

As can be seen from the form of this equation for $\Psi(x)$, ξ_{GL} is a characteristic length, over which $\Psi(x)$ cannot vary rapidly. It is called the Ginzburg-

16. deGennes, see ref. 5, p. 178.

Landau coherence length and, near T_c , has the temperature dependence,¹⁷

$$\xi_{GL}(T) = 0.74 \xi_0 [T_c / (T_c - T)]^{\frac{1}{2}} \quad \text{I.E.15}$$

(for a pure metal)

$$\xi_{GL}(T) = 0.85 [\xi_0 \& T_c / (T_c - T)]^{\frac{1}{2}} \quad \text{I.E.16}$$

(for a dirty metal)

A dirty metal is one in which the mean-free-path is much less than the coherence length.

II. Theory of the Experiment.

II.A. The Ginzburg-Landau Theory Applied to N-S Junctions.

The G-L theory allows one to find the order parameter in a superconductor when the superconductor borders on a normal (an S-N interface) metal. Consider the one-dimensional problem of a normal metal (occupying the half-space $-\infty < x < 0$) in contact with a superconductor

17. deGennes, see ref. 5, p.225.

(occupying the half-space $0 < x < \infty$) at the plane $x = 0$. The solution¹⁸ to Eq. I.E.13 is,

$$\Psi(x) = \tanh[(x - x_0)/\sqrt{2} \xi_{GL}] \quad \text{II.A.1}$$

The quantity x_0 must be chosen to satisfy the boundary condition given by Eq. I.E.8. This can be written,

$$\nabla_n \Psi = d\Psi/dx \big|_{x=0} = \Psi/b \quad \text{II.A.2}$$

where \hbar and $\psi_0 = (-\beta/\alpha)^{\frac{1}{2}}$ have been absorbed into the constant $1/b$. Then b determines the magnitude of Ψ at the boundary. It is usually called the extrapolation length.¹⁸ If $x_0 \ll \xi_{GL}$, then $-x_0 \simeq b$. The solution for $\Psi(x)$ also satisfies the boundary condition at $x \rightarrow \infty$ (see Eq. I.E.7).

In Fig. 2 a plot of $\Psi(x)$ vs. x is shown. The value of b has been chosen as $0.2 \xi_{GL}$. The value of $\Psi(x)$ at the boundary $x = 0$ may be closely approximated by assuming that,

18. deGennes, see ref. 5, p.233.

$$\Psi(x=0) = b/\sqrt{2} \xi_{GL} \quad \text{II.A.3}$$

It is shown in Fig. 2 that,

$$\Psi(x) = [1/(b + \sqrt{2} \xi_{GL})]x + (b/\sqrt{2} \xi_{GL}) \quad \text{II.A.4}$$

is a reasonable approximation to Eq. II.A.1.

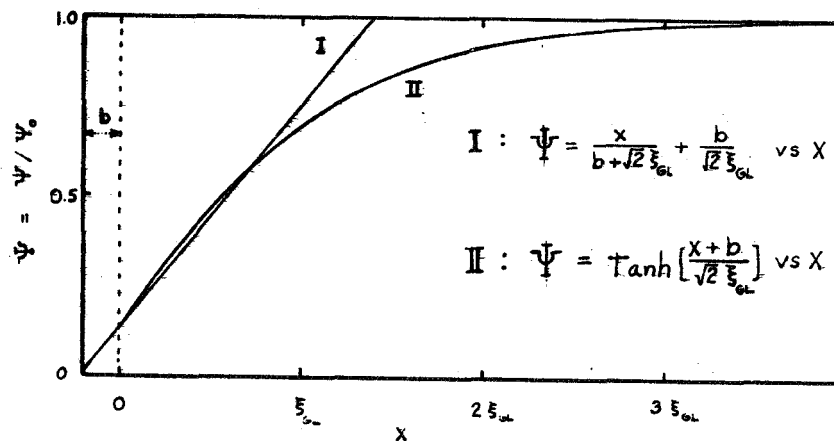


Fig. 2 $\Psi(x)$ vs. x

II.B. The deGennes Theory of an N-S Junction.

To find the order parameter in a normal metal, near

an N-S boundary, a theory of deGennes¹⁹ is used.

A "condensation amplitude", $F(x)$, is defined by deGennes as,

$$F(x) = \langle \hat{\psi}_{\uparrow}(x) \hat{\psi}_{\downarrow}(x) \rangle \quad \text{II.B.1}$$

where $\hat{\psi}_{\uparrow}(x)$ and $\hat{\psi}_{\downarrow}(x)$ are annihilation operators for an electron with spin up and spin down, respectively. $F(x)$ denotes the probability amplitude for finding two electrons in the condensed state at the point x . Then, $\psi(x)$ can be replaced by $F(x)$ in the following work.

$F(x)$ is related to the energy gap by the expression, $\Delta(x) = V(x)F(x)$. $V(x)$ is the interaction potential. $\Delta(x)$ is a spatially dependent energy gap function, first introduced by Gor'kov²⁰⁻²² in his microscopic derivation of the G-L equations. It is called the pair potential.

19. P.G. deGennes, Rev. Mod. Phys. 36, 224 (1964).
20. L.P. Gor'kov, J.E.T.P. 36, 1918; 37, 833, 1407; Soviet Physics JETP 9, 1364 (1959).
21. L.P. Gor'kov, J.E.T.P. 34, 735; Soviet Physics JETP 7, 505 (1958).
22. L.P. Gor'kov, Soviet Physics JETP 10, 593, 998 (1960).

According to Deutscher and deGennes²³, the behavior of $F(x) = F_N(x)$ in the normal metal is given by,

$$F_N(x) = \Lambda(x) \exp(-K|x|) \quad \text{II.B.2}$$

for $|x| > K^{-1}$. $\Lambda(x)$ is a slowly varying function of x (the distance from the boundary) and can be neglected compared to the exponential term. If the normal metal has a transition temperature, T_{cN} , then for $T_{cN} \geq 0$, K^{-1} is given by,²⁴

$$K^{-1} = \xi_N [1 + 2/\ln(T/T_{cN})] \quad \text{II.B.3}$$

ξ_N is the coherence length in the normal metal and is given by,²³

$$\xi_N = \hbar v_N / 2\pi kT \quad \text{in the clean limit} \quad \text{II.B.4}$$

and,

$$\xi_N = (\hbar v_N \ell_N / 6\pi kT)^{\frac{1}{2}} \quad \text{in the dirty limit} \quad \text{II.B.5}$$

23. G. Deutscher and P.G. deGennes, see ref. 14, p.1006.

24. J. Clarke, Proc. Roy. Soc. A308, 447 (1969).

Two other boundary conditions^{16,25} to be met at the N-S interface are,

$$F_N(0)/N_N = F_S(0)/N_S \quad \text{II.B.6}$$

and

$$v_N \ell_N \left. \frac{dF_N(x)}{dx} \right|_{x=0} = v_S \ell_S \left. \frac{dF_S(x)}{dx} \right|_{x=0} \quad \text{II.B.7}$$

where N_S and N_N are the respective densities of state (at the Fermi surface) in the S and N materials. F_S is the value of F in the superconductor. It will be assumed that $N_S = N_N$ so that,

$$F_N(0) = F_S(0) \equiv F(0) \quad \text{II.B.8}$$

Then Eq. II.A.3 becomes,

$$F(0)/F_S(\infty) = b/\sqrt{2} \xi_{GL} \quad \text{II.B.9}$$

and Eq. II.B.2 can be approximated by,

25. N.R. Werthamer, Phys. Rev. 132, 2440 (1963).

$$F_N(x) = [F_S(\infty)b/\sqrt{2} \xi_{GL}] \exp(-|x|/\xi_N) \quad \text{II.B.10}$$

where T_{cN} is assumed to be zero. On the S side of the interface, Eq. II.A.4 becomes,

$$F_S(x) = F_S(\infty)x/(b + \sqrt{2} \xi_{GL}) + F_S(\infty)b/\sqrt{2} \xi_{GL} \quad \text{II.B.11}$$

for $0 < x < \sqrt{2} \xi_{GL}$ and,

$$F_S(x) = F_S(\infty) \quad \text{II.B.12}$$

for $x > \sqrt{2} \xi_{GL}$. From Eq. II.B.7, the extrapolation length is given by,

$$b = v_S \ell_S \xi_N / v_N \ell_N \quad \text{II.B.13}$$

The condensation amplitude has now been determined in the vicinity of an N-S boundary.

II.C. The Josephson Effect.

The fact that supercurrents can pass through a thin layer of non-superconducting material, sandwiched between two superconductors, was experimentally discovered by H. Meissner²⁶. Four years later, Josephson²⁷ wrote a theoretical paper explaining the superconducting tunneling of Cooper pairs and predicting other effects such as a.c. (alternating current) supercurrents at finite voltages, d.c. (direct current) current steps in r.f. (radio frequency) fields and magnetic interference.

Josephson used the method of the tunneling Hamiltonian, in which the transfer of normal electrons is the primary process. He then showed that a secondary process, which had previously escaped notice, was the transfer of electron pairs, giving rise to a supercurrent. In the original paper, it was noted that the non-superconducting material could be either an insulator or a normal metal. However, most of the following work was with insulators

26. H. Meissner, Phys. Rev. 109, 686 (1958).

27. B.D. Josephson, Phys. Letters 1, 251 (1962).

and only the SIS (superconductor-insulator-superconductor) junction is widely known as a "Josephson junction". The SNS (superconductor-normal metal-superconductor) junction is, in fact, quite similar to the SIS junction. The primary differences are in the magnitude of the supercurrents (commonly called Josephson currents), their temperature dependence and, at finite voltages, the co-existence of large normal currents. A wave-mechanical derivation of the Josephson effect, based on the G-L theory will be presented here.

In the presence of a small current, the complex nature of the condensation amplitude $F = |F| \exp(i\Theta)$ must be considered. The absolute phase Θ is undetermined by the G-L equations. That is, if F_1 is a solution to the G-L equations, then $F_1 \exp(i\Theta)$ is also a solution. However, phase differences in superconductors are determined in these equations. The fact that phase differences are determined implies that the phase is a variable having the property of long-range-order. As pointed out by Anderson²⁸, the phase is both a thermodynamic and a dynamic variable, with a time dependence,

28. P.W. Anderson, Rev.Mod.Phys. 38, 298 (1966).

$$\hbar d\theta/dt = \partial G/\partial n = \mu = qV \quad \text{II.C.1}$$

where G is the free energy, q is the charge ($q = 2e$ for a Cooper pair), n is the number of particles described by θ and μ is the chemical potential. This relation, with $q = 2e$, is also known as the Josephson frequency relation.

The long-range-order in θ is due to the interactions of the electrons in the superconductor. If two superconductors are physically separated, the motion of the electrons in one are independent of the motion in the other. Then θ_1 in one superconductor is not correlated with θ_2 in the other. If the two superconductors are brought together in such a manner as to allow a small fraction of the electrons in one to flow to the other, the phases may become correlated, if not equal. This is called weak-coupling. Methods of producing weak-coupling include the placing of a thin layer of normal metal, a very thin layer of oxide or a narrow superconducting bridge between the two superconductors. The microscopic theory shows that the supercurrent (Josephson current), that may pass through such a weak-link, has the phase dependence,

$$I_s = I_m \sin(\theta_2 - \theta_1) \quad \text{II.C.2}$$

where I_m is a parameter to be discussed.

The derivation of Eq. II.C.2, from deGennes' theory of an SNS junction¹⁹, depends on the microscopic result that F_N decays exponentially with distance in the normal metal. Consider the SNS junction shown in Fig. 3.

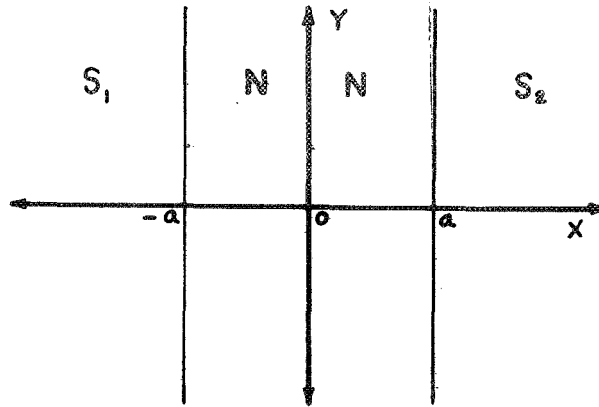


Fig. 3 A Model
of an SNS junction.

The condensation amplitude, evaluated in the normal metal, has a contribution from each superconductor. Assuming that the two superconductors are identical, so that $F_S(\infty)$ is the same in each, Eq. II.B.10 becomes,

$$F_N(x) = [F_S(\infty) b / \sqrt{2} \xi_L] \times \left\{ \exp[-(x + a)/\xi_N + i\theta_1] + \exp[(x - a)/\xi_N + i\theta_2] \right\} \quad \text{II.C.3}$$

where θ_1 and θ_2 are the phases in the superconductors on each side of the normal metal. The factor $\pm a$ has been added to obtain the proper boundary conditions at the interfaces ($x = \pm a$). The total thickness of the normal is, $\delta_N = 2a$.

To obtain the Josephson supercurrent density, j_S , use is made of Eq. I.E.6. For small (or zero) magnetic fields, it becomes,

$$j_S = (e\hbar/mi)(F^*dF/dx - FdF^*/dx) \quad \text{II.C.4}$$

Making the substitution for $F_N(x)$ given by Eq.II.C.3, the x dependence drops out and j_S becomes,

$$j_S = j_c \sin(\theta_2 - \theta_1) \quad \text{II.C.5}$$

with j_c given by,

$$j_c = \frac{2v_s^2 \ell_s^2 e \hbar |F_S(\infty)|^2 \xi_N}{v_N^2 \ell_N^2 m \xi_{GL}^2} \exp(-\delta_N / \xi_N) \quad \text{II.C.6}$$

Eq.II.B.13 has been substituted for b. It can be seen that the supercurrent density depends exponentially on the normal metal thickness, $2a$.

j_c is called the critical Josephson current density. It is temperature dependent, as can be seen by examining ξ_N . ξ_{GL} is given by Eq.I.E.15, and ξ_N is given by Eq.II.B.5. The temperature dependence of $F_S(\infty)$ is the same as that of the energy gap²⁹. Making these substitutions, and introducing the reduced temperature, $t = T/T_c$, and a reduced energy gap, $\Delta(t)/\Delta(0)$, it is found that,

$$j_c(t) = D[\Delta(t)/\Delta(0)]^2 t^{-\frac{1}{2}}(1 - t) \exp(-\delta_N / \xi_N) \quad \text{II.C.7}$$

with a temperature independent quantity, D , given by,

$$D = \frac{2v_s^2 \ell_s^2 e \hbar \Delta^2(0) (\hbar v_N \ell_N)^{\frac{1}{2}}}{m v_N^2 \ell_N^2 V^2 (6\pi k T_c)^{\frac{1}{2}} (0.55 \xi_0^2)} \quad \text{II.C.8}$$

29. G. Rickayzen, see ref. 14, p.75.

It is convenient to look at the $\ln j_c$, given by,

$$\ln j_c(t) = C_0 + f(t) - \delta_N (6\pi kT_c / \hbar v_N \ell_N)^{\frac{1}{2}} t^{\frac{1}{2}} \quad \text{II.C.9}$$

Where $C_0 = \ln D$, and,

$$f(t) = \ln [\Delta(t)/\Delta(0)]^2 t^{-\frac{1}{2}} (1-t) \quad \text{II.C.10}$$

$f(t)$ has been calculated and plotted vs t in Fig. 4.

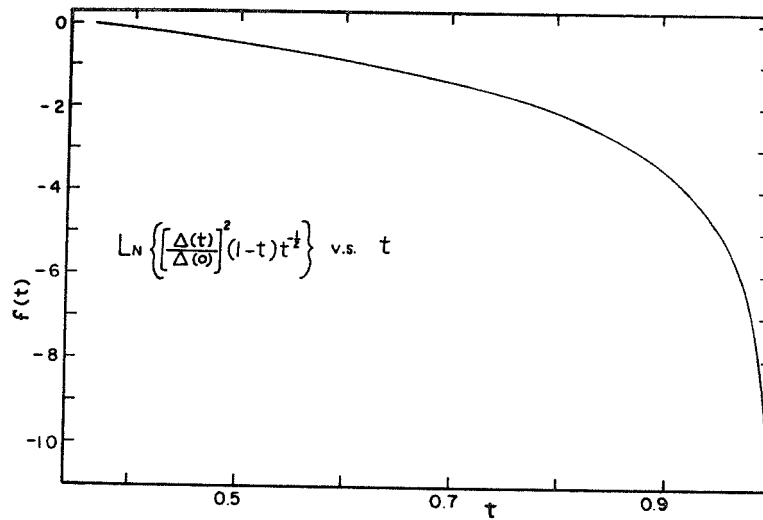


Fig. 4 $f(t)$ vs t .

Near T_c , $\Delta(t)$ varies as $(1-t)^{\frac{1}{2}}$ and $t^{\frac{1}{2}}$ variations are negligible. Then $j_c(t)$ has the dependence,

$$j_c(t) \propto (1 - t)^2 \quad \text{for } t \sim 1 \quad \text{II.C.11}$$

For low temperatures, $\Delta(t)$ does not vary rapidly and the exponential term in $j_c(t)$ will dominate. That is,

$$\ln j_c(t) \propto -t^{\frac{1}{2}} \quad \text{for } t \ll 1 \quad \text{II.C.12}$$

For intermediate temperatures, the complete expression derived for $j_c(t)$ must be used.

II.D. Magnetic Properties of the Josephson Junction.

II.D.1. Quantum Interference.

In a magnetic field, the phase difference of the condensation amplitude, across a barrier, is not an invariant quantity. To make it so,^{30,31} a factor of $(-2e/\hbar c) \int_1^2 A \cdot dl$ must be added so that,

30. P.W. Anderson and J.M. Rowell, Phys. Rev. Let. 10, 230 (1963).

31. B.D. Josephson, Rev. Mod. Phys. 36, 216 (1964).

$$F(x,A) = F(x,0) \exp\left[(-2ie/\hbar c) \int_1^2 A_x dx\right] \quad \text{II.D.1}$$

The effects of a magnetic field upon a Josephson junction were first observed by Rowell³². They are direct proof of quantum interference on a macroscopic scale. The effect may be calculated as follows.³³

Consider the two-dimensional junction shown in Fig.5.

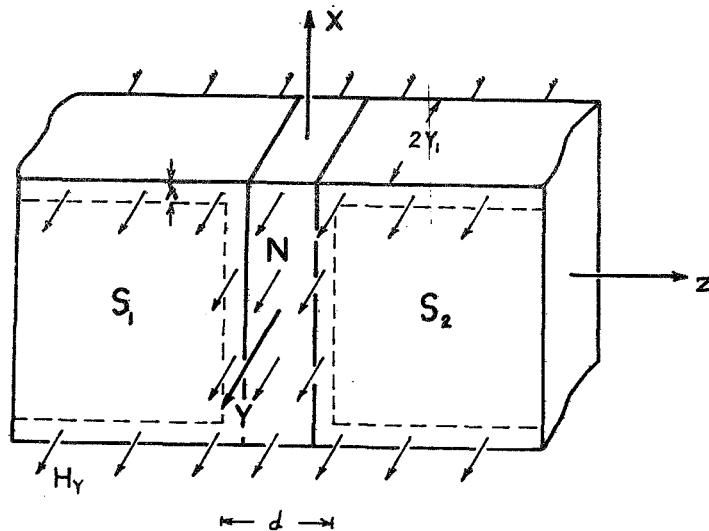


Fig. 5 A Two Dimensional SNS Junction
in an Applied, Normal Magnetic Field, H_y .

-
32. J.M. Rowell, Phys. Rev. Let. 11, 200 (1963).
 33. R.P. Feynman, R.B. Leighton and M. Sands, Lectures on Physics (Addison-Wesley, Mass. 1964) Vol.III, Ch.21.

The total supercurrent, I_s , through the junction, is given by,

$$I_s = \int_{\text{area}}^{\text{barrier}} j_c \sin[\theta_1 + \theta_2 - \frac{2e}{\hbar c} \int_1^2 A_z dz] dx dy$$

II.D.2

where the line integral is evaluated over the distance $d = \phi_N + 2\lambda$. λ is the penetration depth. The current carrying area of the junction is just $2x_1 2y_1$. The line integral becomes $H_y x d$. Then, introducing the quantum unit of flux, Φ_0 ,*

$$\Phi_0 = \hbar c / 2e \quad \text{II.D.3}$$

the supercurrent can be expressed as,

$$I_s = \int_{\text{area}}^{\text{barrier}} j_c \sin[\theta_2 - \theta_1 + (2\pi H_y x d / \Phi_0)] dx dy \quad \text{II.D.4}$$

*In the CGS system, Φ_0 has the value, 2.07×10^{-7} gauss-cm². In the MKS system, $\Phi_0 = \hbar / 2e$ and has the value, 2.07×10^{-15} webers.

This can be rewritten in terms of exponentials as,

$$I_s = j_c \Im [\exp[i(\theta_2 - \theta_1)] \int_{-x_1, -y_1}^{x_1, y_1} \exp(2\pi H_y x d / \Phi_0) dx dy] \quad \text{II.D.5}$$

where \Im means "the imaginary part of". Performing the integration and multiplying by $1 = 2x_1/2x_1$, this becomes,

$$I_s = j_c \frac{2x_1 2y_1}{2\pi x_1 H_y d / \Phi_0} \sin(\theta_2 - \theta_1) \sin(2\pi H_y x_1 d / \Phi_0) \quad \text{II.D.6}$$

Noting that $2x_1 H_y d$ is the magnetic flux Φ , through the junction, and inserting absolute value signs, since the direction of current flow depends on external conditions, the supercurrent becomes,

$$I_s = I_m \sin(\theta_2 - \theta_1) \quad \text{II.D.7}$$

where,

$$I_m = I_c \sin(\pi \Phi / \Phi_0) / (\pi \Phi / \Phi_0) \quad \text{II.D.8}$$

and I_c is the critical Josephson current and I_m is a maximum critical Josephson current.

Another case of interest is that of two similar

Josephson junctions in parallel. The circuit is illustrated in Fig.6.

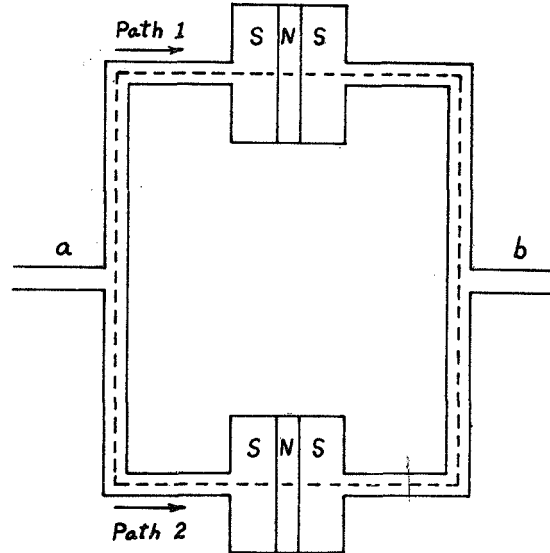


Fig.6 Two Josephson Junctions in Parallel.

The condensation amplitude is again given by Eq.IID.1 and the difference in amplitude between points a and b must be independent of the path taken for the line integral. Performing the integration³³, it is found that

$$I_m = 2I_c \left| \frac{\sin(\pi \Phi / \Phi_0)}{(\pi \Phi / \Phi_0)} \right| \left| \cos(\pi \Phi / \Phi_0) \right| \quad \text{II.D.9}$$

where I_c is the critical Josephson current of the individual junctions and I_m is the total maximum Josephson current. Φ is the magnetic flux passing through each junction and Φ_T is the total magnetic flux enclosed between the two junctions. This is a quantum interference effect and was first seen by Jaklevic, Lambe and Silver³⁴. The double junction is pertinent to this work because multiple junctions may arise in mechanical contacts. The experimental results verify this.

II.D.2. The Josephson Penetration Depth.

It has been shown by Ferrell and Prange³⁵ that the magnetic field of a supercurrent, flowing through a Josephson junction, exhibits a Meissner effect which in turn limits the maximum current. This is called self-field limiting. The characteristic length of the magnetic field penetration into the junction is,

$$\lambda_J = (\hbar c^2 / 8\pi I_c e d)^{\frac{1}{2}} \quad \text{II.D.10}$$

34. R.C. Jaklevic, J.J. Lambe and A.H. Silver, Phys. Rev. Let. 12, 159 (1964).

35. R.A. Ferrell and R.E. Prange, Phys. Rev. Let. 10, 479 (1963).

λ_J is called the Josephson penetration depth. As defined in Fig.5, $d = \delta_N + 2\lambda$. Thus, if the width of the junction is less than λ_J , we can assume that the current is evenly distributed throughout the junction. However, if the width is much greater than λ_J , the current will be confined to the area within a distance λ_J from the edge of the junction. These results are approximate, as the problem has not been solved exactly for a finite geometry. Typically, λ_J is of the order of 0.1mm.

II.E. Electrical Characteristics of the Josephson Junction.

II.E.1. Current-Voltage Characteristics.

When the current flowing through a Josephson junction is less than the maximum critical current, Eq.II.D.7 is applicable and there is no voltage across the junction. When I_m is exceeded, a voltage will appear and the characteristics of the junction will be modified.

In the presence of a voltage, the condensation amplitude becomes,³⁶

36. Feynman et.al., see ref. 33, Vol. II, p.15-10.

$$F(x,V) = F(x,0) \exp[(2ie/\hbar c) \int V dt] \quad \text{II.E.1}$$

so that the phase difference across the junction becomes time dependent. The rate of change of this phase difference, $\phi(t)$, is given by,

$$V(t) = (\Phi_0/2\pi) d\phi(t)/dt \quad \text{II.E.2}$$

which is just the Josephson frequency relation given in Eq.II.C.1.

An equivalent circuit for the Josephson junction, driven by a current source, is shown in Fig.7.

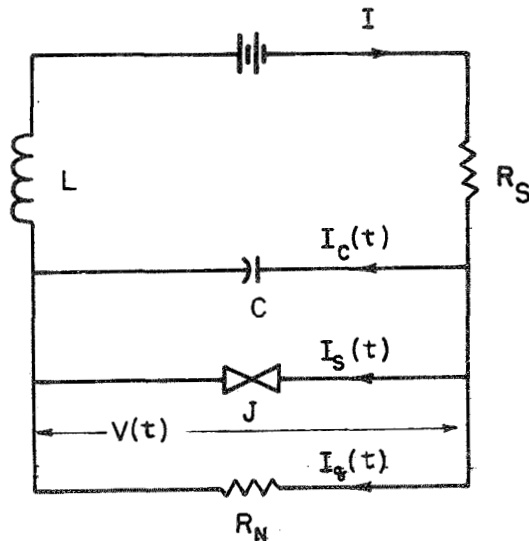


Fig.7 Equivalent Circuit For
A Josephson Junction and Current Source.

The external current, I , is kept constant by a large series resistance, R_S , and an unavoidable lead inductance, L . C is the effective capacitance of the junction and R_N is the resistance of the junction in the normal state.

The time dependent voltage, $V(t)$, excites both a quasi-particle current, $I_q(t)$, and a displacement current, $I_C(t)$. In a two-fluid model,^{4,37} the quasi-particle current corresponds to the normal electron current and can encounter a resistance. It is expected that the resistance would be the same as R_N . The sum of all currents must be,

$$I = I_S(t) + I_q(t) + I_C(t) \quad \text{II.E.3}$$

where the Josephson current is,

$$I_S(t) = I_m \sin \phi(t) \quad \text{II.E.4}$$

the quasi-particle current is,

$$I_q(t) = V(t)/R_N = (\Phi_0/2\pi R_N) d\phi(t)/dt \quad \text{II.E.5}$$

37. J. Bardeen and J.R. Schrieffer, Progress in Low Temp. Physics III (1961), p.70.

and the displacement current is,

$$I_C(t) = (\Phi_0 C / 2\pi) d^2\phi(t)/dt^2 \quad \text{II.E.6}$$

Neglecting the junction capacitance, the total current becomes,

$$I = (\Phi_0 / 2\pi R_N) d\phi(t)/dt + I_m \sin\phi(t) \quad \text{II.E.7}$$

Solving for $\phi(t)$ and using Eq.II.E.2 , it is found that $V(t)$ varies rapidly with time but always remains positive. An externally connected voltmeter measures the time-average given by,

$$V/I_m R_N = [1 - (I_m/I)^2]^{1/2} \quad \text{II.E.8}$$

This relation was developed by Stewart³⁸ and is plotted, in reduced coordinates, in Fig.8.

38. W.C. Stewart, Applied Physics Letters 12, 277 (1968).

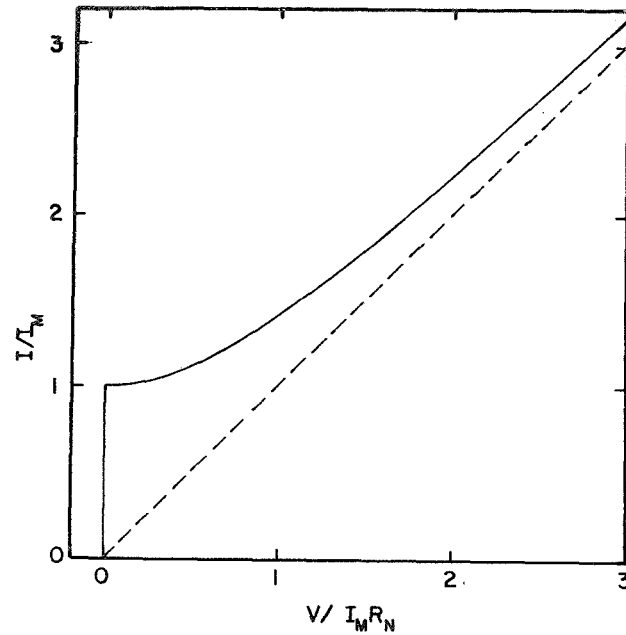


Fig.8 Reduced Current-Voltage Characteristics of a Josephson Junction (from Stewart's theory).

II.E.2. Fluctuations.

The calculations above neglect the effects of fluctuations. If these are large enough, they can modify the current-voltage characteristics and completely decouple the phases across the normal metal barrier.

To consider the effect of fluctuations on the current-voltage characteristics we must add a new, time-dependent current to the differential equation, Eq.II.E.7.

It becomes,

$$I = (\mathcal{E}_0/2\pi R_N) d\phi(t)/dt + I_m \sin\phi(t) + L(t) \quad \text{II.E.9}$$

where $L(t)$ is a fluctuating noise current. Ivanchenko and Zil'berman³⁹ and Ambegaokar and Halperin⁴⁰ have solved this equation by converting it into a Fokker-Planck equation. The resulting integral form is,

$$\begin{aligned} V/I_m R_N = (4\pi/\gamma) \Big\{ [\exp(I\pi\gamma/I_m) - 1]^{-1} \Big[\int_0^{2\pi} g(\phi) d\phi \Big] \Big[\int_0^{2\pi} g^{-1}(\phi') d\phi' \Big] \\ + \int_0^{2\pi} d\phi \int_0^{2\pi} d\phi' g(\phi)/g(\phi') \Big\}^{-1} \end{aligned} \quad \text{II.E.10}$$

where $g(\phi) = \exp[U(\phi)/T]$ and $U(\phi) = \frac{1}{2}T\gamma[(I/I_m) + \cos\phi]$ and,

$$\gamma = \hbar I_m / ekT \quad \text{II.E.11}$$

Ambegaokar and Halperin have performed this integration numerically, and the results are reproduced in Fig.9.

39. Y.M. Ivanchenko and L.A. Zil'berman, Exp. i. Teor. Fiz. 55, 2395 (1968).

40. V. Ambegaokar and B.I. Halperin, Phys. Rev. Let. 22, 1364 (1969).

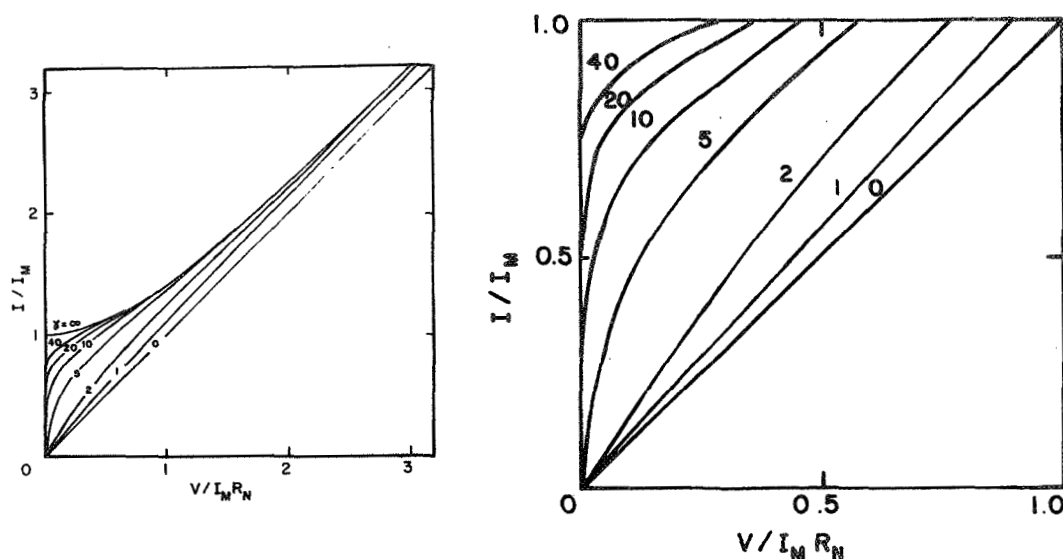


Fig.9 Reduced Current-Voltage Characteristics of a Josephson Junction with Noise Fluctuations.

The coordinates are those of a reduced current and voltage. γ is a parameter which indicates the degree to which the fluctuations produce an effect on the characteristics. In the limit, as γ approaches infinity, the fluctuations produce a negligible effect. In this limit, the characteristics obtained are identical to those obtained by Stewart (Eq.II.E.8).

The results of Ivanchenko and Zil'berman are identical to those found above. In their analysis, the source

of fluctuations was noise in the external circuit, represented by a temperature, T_f , greater than the junction temperature. These effects have been observed here.

II.E.3. Current Steps in the I-V Characteristics.

If an r.f. electromagnetic field is applied to a Josephson junction, current steps can appear in the I-V characteristics under certain conditions. If, in addition to the field, a d.c. voltage, V_0 , given by,

$$V_0 = (\Phi_0 \omega / 2\pi) \quad \text{II.E.12}$$

is biasing the junction, a step will occur. ω is the frequency of the r.f. field. This follows from Eqs. II.E.1 and II.E.4 if one substitutes an r.f. voltage $V_1 \cos \omega t$ for V .³³ The steps also occur for voltages corresponding to harmonics of ω , and were first observed by Shapiro⁴¹.

41. S. Shapiro, Phys. Rev. Lett. 11, 80 (1963).

II.E.4. The Dependence of Voltage on Magnetic Fields.

As shown by Eq.II.D.8, the maximum critical Josephson current depends on the magnetic flux, passing through the junction. This flux is,

$$\Phi = 2\pi r H d \quad \text{II.E.13}$$

where r is the radius of the junction (assuming a circular contact), $d = \delta_N + 2\lambda$, δ_N is the thickness of the normal metal barrier, and $2\pi r d$ is the cross-sectional area, normal to the flow of current.

A convenient expression for the reduced voltage can be found by substituting Eq.II.D.8 into Eq.II.E.8. The result is,

$$V/I_m R_N = \left[(I/I_m)^2 - (\Phi_0/2\pi r H d)^2 \sin^2(2\pi r H d/\Phi_0) \right]^{\frac{1}{2}} \quad \text{II.E.14}$$

In Fig.10, an example of Eq.II.E.14 is plotted in terms of the reduced coordinates, $V/I_m R_N$ and $2\pi r H d/\Phi_0$. A value of $I = 1.1 I_m$ has been chosen for the current.

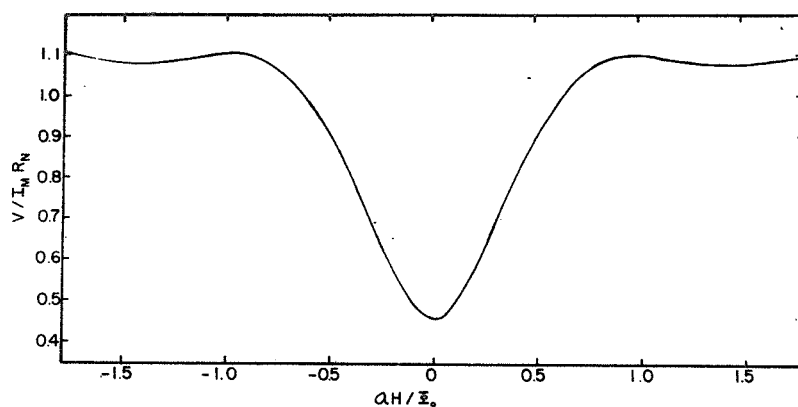


Fig.10 Voltage Across the
Junction vs Magnetic Field.

In practice, when a mechanical contact is made between two crossed wires, it is likely that the contact will be formed in more than one location⁴². Fig.11 represents a

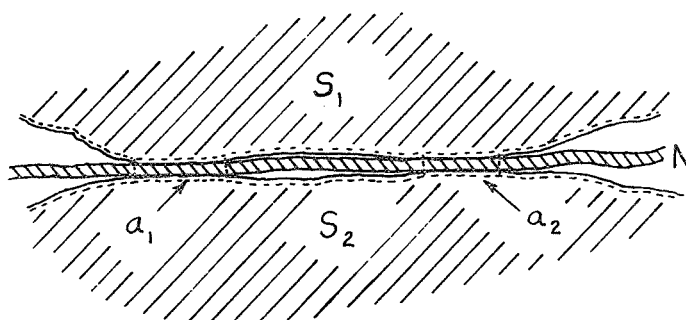


Fig.11 A Hypothetical
Mechanical Contact.

42. J.E. Zimmerman and A.H. Silver, Phys. Rev. 141, 367 (1966).

a possible configuration of such a situation. The dotted lines represent the penetration depth.

Under these circumstances, there are two or more Josephson junctions in parallel and the V-H characteristics will be changed. They may be obtained by substituting Eq.II.D.9 into Eq.II.E.8. The result is,

$$V/I_m R_N = [(I/I_m)^2 - (\Phi_0/\pi a H)^2 \cos^2(\pi a_r H/\Phi_0) \sin^2(\pi a H/\Phi_0)]^{\frac{1}{2}}$$

II.E.15

where a is the cross-sectional area of each junction and a_r is the cross-sectional area enclosed by both junctions (a double contact). Eq.II.E.15 is plotted in Fig.12 in terms of reduced coordinates. A value of $I = 1.1I_m$ has been chosen for the current.

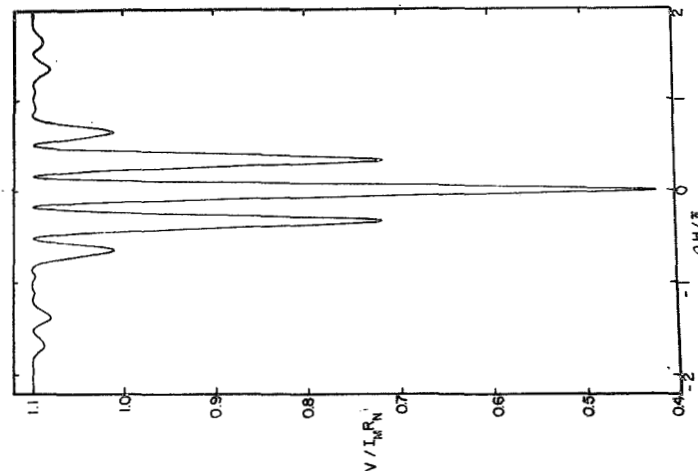


Fig.12 Voltage Across a Double Contact Junction vs Magnetic Field.

III. Description of the Experiment.

III. A. Introduction.

The purpose of this experiment was to measure the electrical characteristics of the SNS mechanical-contact junction as a function of temperature, magnetic field and normal metal parameters (where one hoped to work in both the clean and dirty limits of the normal metal). It was also desired to introduce a second current, by means of the normal metal, directly into the junction area and observe the effects on the I-V characteristics.

When this work was started, there was no experimental evidence that an SNS contact behaved as a Josephson junction. Previous experiments^{26,43} had shown that supercurrents would pass through such a junction if δ_N were thin enough ($\delta_N \approx 3000$ angstroms) but the theoretical basis for this effect was not known at that time. The behavior of an SNS junction had not been studied in a magnetic field and the inherent noisiness of the contact made the

43. H. Meissner, Studies of Contacts With Barriers in Between, ONR Report Nonr. 248 (49), 1959.

determination of critical currents near T_c very difficult. The functional dependence of the critical current upon the normal resistance of the junction was unknown and results seemed to indicate that the current carrying area of the junction was three or four orders of magnitude less than the load bearing area.

The study of SNS mechanical contacts are of interest because it allows the control of the parameters of the normal metal and superconductor. Other junction forming techniques, such as vapor deposition of the metals in sequence, alter the properties of the material. For instance, it is known that⁴⁴ the density of copper films, deposited at 77K, have a density of only 2/3 of their bulk value. In addition, diffusion between the metals can be a serious problem unless the deposition is carried out at low temperatures.

The SNS Josephson junction is also of interest because of the possible device applications. The low resistance of the normal metal (as opposed to the SIS

44. A. v. Bassewitz and G. v. Minnigerode, Z. Physik 181, 368 (1964).

Josephson junction) allows much higher critical currents and, as mentioned, provides a third terminal for possible control applications.

In these experiments, gold was chosen as the normal metal. It is useful because it does not oxidize, it has a low resistivity and can readily be grown as a single crystal. The superconductor was tin. A mechanical, crossed-wire contact was formed at 4.2K, under a controlled force. The gold (either electroplated or in the form of a single crystal) was sandwiched between the tin wires.

III.B. The Cryostat.

The cryostat consisted of a glass dewar (containing the experimental apparatus) supported within a cylindrical brass can. The latter is connected to a mounting plate and vacuum line. The brass can is placed in a metal dewar containing liquid nitrogen, such that the top of the can stays at 77K. This reduces heat flow into the cryostat.

The brass can is connected to the mounting plate

and sealed with an o-ring. The vacuum line leads to a Kinney KS-47 mechanical pump. The helium bath temperature can be varied from 4.2K to 1.4K by pumping on its vapor. The pressure is measured with a mercury-filled U-tube manometer. The corresponding temperature is found in the NBS 1958 Helium Vapor Pressure-Temperature Scale Table⁴⁵. Pressures are read to an accuracy of ± 0.2 mm, corresponding to an accuracy of a fraction of a millidegree at 3.7K and to several millidegrees at 1.4K.

The metal construction of the cryostat shields the interior of the dewar from most r.f radiation. However, it is possible for some radiation to enter the cryostat through a few un-shielded leads so that our experiment is not completely r.f field free.

Non-magnetic materials are used in the construction so as to allow the penetration of externally applied magnetic fields. In particular, we must be able to compensate for the earth's magnetic field.

45. National Bureau of Standards Monograph 10 (June 1960).

The temperature of the helium bath is stabilized at any desired point with a phase-sensitive temperature controller *, a manganin wire heating element and a carbon resistor thermometer. Allan-Bradley carbon composition resistors (100 ohm) are also used as level detectors in the cryostat.

Stray magnetic fields, including that of the earth's, must be compensated at the location of the experiment. This is accomplished with an external Helmholtz coil.

III.C. The Sample Holder.

The purpose of the sample holder is to support the superconducting tin wires and the gold film mounted between them. It must also keep them separated until they are cooled to 4K.

The sample holder is mounted in the cryostat as shown in Fig.13. A spring-loaded tensioning device is mounted on the top of the cryostat and a cord passes down to a leaf spring on the sample holder. The force is variable.

* Designed and built by H. Meissner.

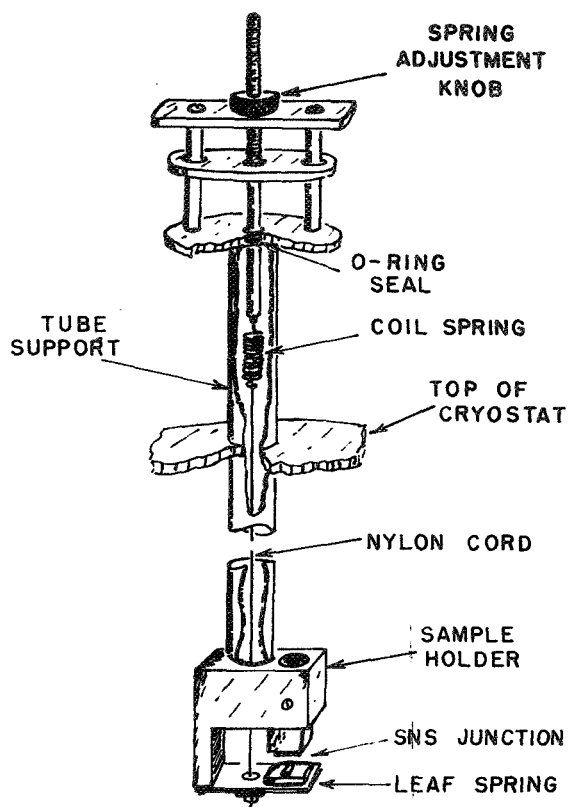


Fig.13 A cut-away view of the cryostat and sample-holder mount

The sample-holder is shown, in more detail, in Fig.14. The hole seen on the top at the left, is for the support tube. It also allows the passage of the cord to the leaf spring. The other hole is for the upper tin wire holder. This holder may be moved up and down for proper height adjustment. On the bottom of the sample-holder, there is a phosphor-bronze leaf spring. One of the tin wires is mounted on a phenolic sheet, which is fixed to the

spring. The other is mounted, at right angles, above it. The wires may be positioned with a fraction of a millimeter separating them. When desired, the leaf spring may be drawn up and contact made under a controlled force.

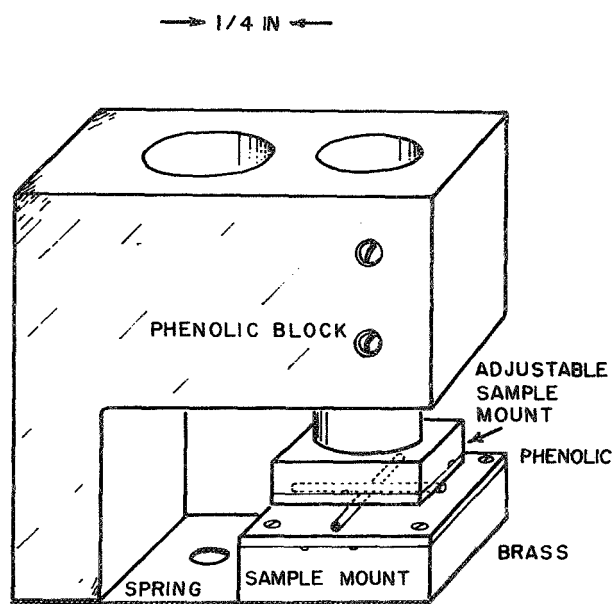


Fig.14 Sample-Holder

The crossed-wire geometry of the contact is shown in Fig.15 (tin-electroplated gold-tin) and Fig.16 (tin-electroplated gold + gold film-tin). The current and potential leads are arranged in standard "H" pattern. Originally, the leads were soldered directly to the tin wires. However, it was felt that this might allow super-current loops, with disruptive magnetic fields, to form

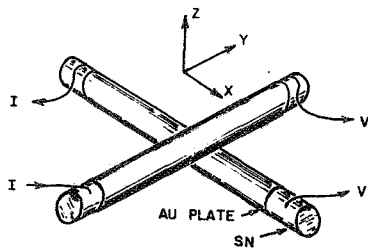


Fig.15 SNS Contact
With Plated Gold.

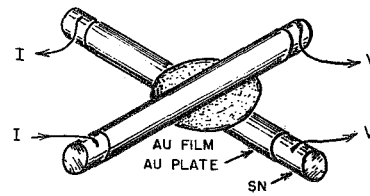


Fig.16 SNS Contact
With Gold Film.

at the connection. In later experiments, the connection was made by means of brass screws with leads epoxied to them. When a second current was passed through the junction, the lead was attached directly to the gold film by means of a wire hoop supporting the film.

When a gold film was used in the experiment, it was positioned over one of the tin wires, as shown in Fig.17. The film is suspended on a copper wire hoop that is attached to the spring-loaded adjusting mechanism shown. This device is made from brass, incorporates a stainless steel (non-magnetic) coil spring and an 0-80 brass screw to vary the height of the hoop.

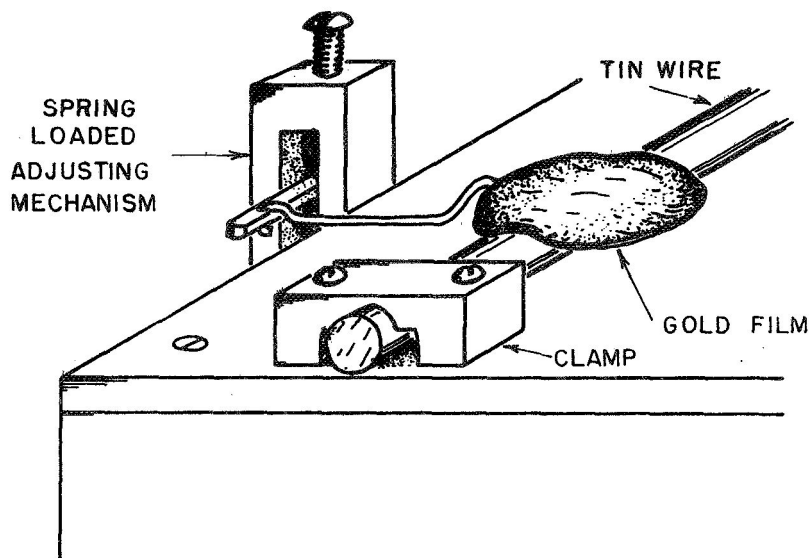


Fig.17 Arrangement For
Positioning The Gold Film.

III.D. Sample Preparation.

It was originally intended that a gold film, with a long electronic mean-free-path, be positioned between two bare tin wires. The large coherence length of the gold would then permit superconducting tunneling over comparatively large distances. Extensive experiments with this arrangement proved that the technique was not feasible. An oxide layer builds up on the tin and the resulting barrier decouples the two superconductors, preventing tunneling. An exception to this was when no gold film, or an extremely thin gold film, was placed between the

tin. Then, the usual SIS Josephson currents were observed.

A solution to this problem was found by electroplating the tin wires with a thin layer of gold. It was found that 300 angstroms (\AA) or more, of gold, would inhibit the oxidation to a degree that a successful SNS junction could be formed. The technique was to electropolish the tin wire (99.999% pure, extruded to a diameter of 0.325mm) and then, very quickly, rinse and immerse in the electroplating solution. This was done just before the experiment and no more than $1\frac{1}{2}$ hours elapsed before the wires were cooled to 4K. The electroplating solution was an ammonia cyanide (Baker's) solution used at room temperature. The electropolishing solution was perchloric acid (20 parts) and acetic acid (70 parts) kept at 0°C . An EMF of 4 to 5 volts was used. The gold used in the plating process was 99.99% pure.

After plating, the wire was rinsed in three solutions of distilled water and then cleaned ultrasonically in benzene. It was then cut in half and mounted.

With the above technique, the normal resistance of the SNS contacts was found to decrease by two to four orders of magnitude to the 10^{-4} ohm region.

The gold film was prepared by vapor depositing 99.999% pure gold onto a heated, polished salt crystal (NaCl) in a vacuum. The gold film thus formed is a single crystal⁴⁶.

The substrate is prepared by cleaving a large salt crystal, (obtained from the International Salt Co., Clarks Summit, Penn.) and polishing it on a glass blank, covered with filter paper. The paper is impregnated with a paste of distilled water, methanol and aluminum oxide powder (Fisher Alumina Dry Powder, Type B, 1 micron particle size). As the paste becomes dry, it is dampened with a solution of 90% methanol, 10% water. When a good polish is obtained, the crystal, now about 1 inch square and $\frac{1}{4}$ inch thick, is ultrasonically cleaned in benzene and allowed to dry in air.

The crystal is mounted in a bell jar evaporator within 30 minutes of preparation. It is supported with a mask on the bottom and a heat sink on the top. The temperature is controlled with a heat lamp and determined with a thermocouple. The arrangement is shown in Fig.18.

46. J.W. Matthews and E. Grumbaum, Phil. Mag. 11, 1233 (1965).

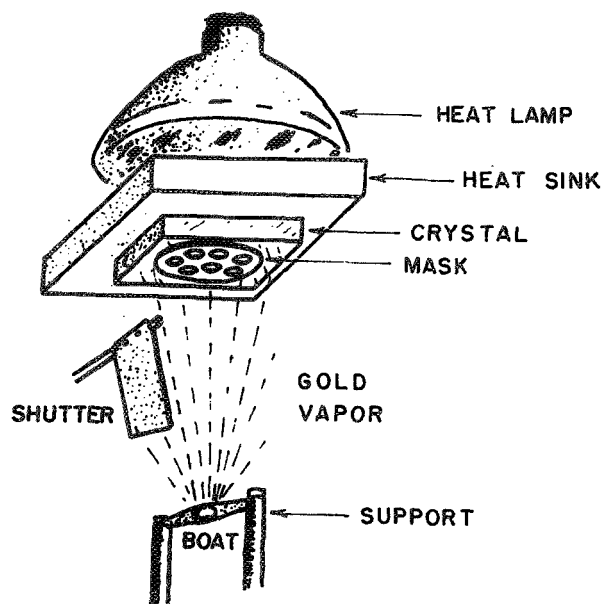


Fig.18 Gold Film
Vapor Deposition Arrangement.

The mask has 3/16 inch diameter holes which provide a convenient gold film size. It also has an H-pattern (not shown) which provides a thickness sample.

After the crystal has been mounted, the system is evacuated and baked out at 160°C for about 18 hours. Then, over a period of several hours, the crystal is heated slowly to prevent cracking from thermal stresses. At a temperature of 410°C the deposition begins. The pressure at this point is about 1×10^{-5} torr. The rate of deposition, from the molybdenum boat, is about 2000 Å/min. At the end of the deposition, the pressure has risen to

5×10^{-5} torr.

When the vapor deposition is complete, the crystal is allowed to cool slowly. It can then be removed and stored for future use. When needed, the gold film is removed from the crystal by floatation in water. The salt dissolves and the film floats off onto the surface. It is picked up with a #38 Cu wire hoop, rinsed in water, methanol, and benzene and mounted for use immediately.

III.E. Magnetic Field Coils.

There are three Helmholtz coils used in the experiment. The first is a large coil used externally and equipped with an azimuth adjustment, to compensate for the earth's magnetic field. The second is also used externally and provides a maximum field of 10 gauss at the sample in the x-direction (see Fig. 15 for a definition of directions). The third is a small niobium wound coil, used inside the cryostat. It was designed and built by P. Tholfsen⁴⁷ and provides a maximum field (in the y-direction) of about 900 gauss at 1.4K. The calibrations of these coils were checked with a Hewlett Packard 428B d.c. milliammeter with #3529A probe.

47. P. Tholfsen, Ph.D. thesis, Stevens Institute of Technology, unpublished (1969).

III.F. Measurements.

III.F.1 Thickness of the Normal Metal.

The thickness of the electroplated layer of gold was determined from the surface area of the tin wire and the application of Faraday's law of electrolysis. A density of 19.3 g/cm^3 was assumed for the gold, and a plating efficiency of 96% was taken into account.

The thickness of the epitaxially grown gold films was determined by optical methods ^{48,49} using the principle of multiple-beam interferometry. The thickness sample was grown on a glass substrate, next to the film. The accuracy of this method was usually better than 50\AA .

III.F.2. The Mean-Free-Path of the Gold.

The mean-free-path of the normal metal can be used in the determination of the coherence length and it indicates whether one is in the clean or dirty limit of the

48. W.F.Koehler, Jour. Opt. Soc. Amer. 43, 739 (1953).

49. R.F.Duffy, Ph.D. thesis, Stevens Institute of Technology, unpublished (1964).

theory. The mean-free-path of the electroplated gold cannot be measured directly and it can not be used to determine ξ_N . That must be determined experimentally.

The mean-free-path of the single crystal gold films can be determined by a method developed by Fuchs⁵⁰ and reviewed by Dingle⁵¹ and Sondheimer⁵².

At liquid helium temperatures, the resistivity of a bulk normal metal is determined, primarily, from its impurities. This is increased for thin films by the boundary scattering of electrons from the relatively large surface area. In order to obtain a bulk value of the mean-free-path, ℓ_0 , it is necessary to eliminate the contribution of the boundary scattering.

The resistance of an H-pattern sample of the gold film is determined at room temperature and 4K. This information, along with the gold thickness, δ_N , the room temperature conductivity, σ_{293} , and the ratio of ℓ_0 to the bulk conductivity σ_0 , will give the value of a

50. K. Fuchs, Proc. Camb. Phil. Soc. 34, 100 (1938).

51. R.B. Dingle, Proc. Roy. Soc. London A201, 545 (1950).

52. E.H. Sondheimer, Advan. in Physics 1, 8 (1952).

constant, K_F , used in the determination of ℓ_0 .

$$K_F = (R_{293}/R_{4.2})(\sigma_{293}/\sigma_N)(\ell_0/\sigma_0) \quad \text{III.F.1}$$

where a value of⁵³ $\sigma_{293} = 4.1 \times 10^5 \text{ ohm}^{-1} \text{cm}^{-1}$ and a value of⁵⁴ $(\ell_0/\sigma_0) = 1.2 \times 10^{-11} \text{ ohm-cm}^2$ is used. From Fuchs' data, a plot of K_F vs σ_N/ℓ_0 can be used to find ℓ_0 . This is plotted in Fig.19.

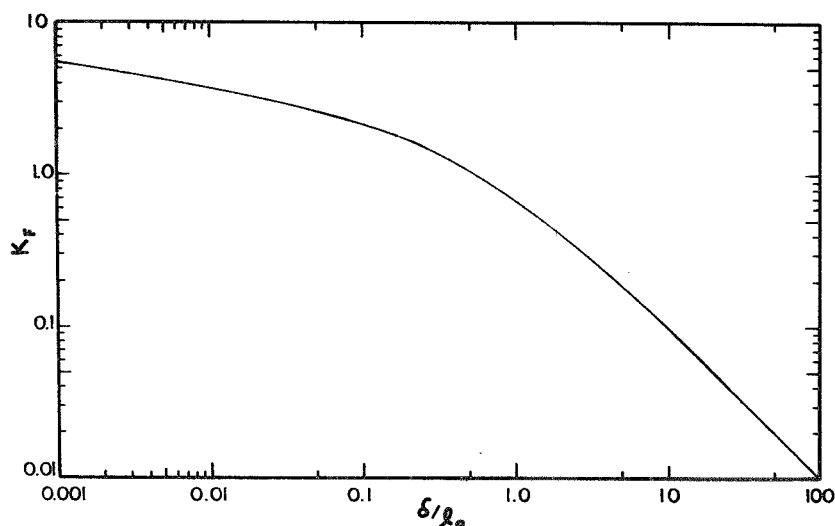


Fig.19 K_F vs σ_N/ℓ_0 .

-
53. Handbook of Physics and Chemistry, 36 (1954-1955).
 54. McDonald, Encycl. Phys., XIV (Springer-Berlin, 1956) p.188.

The experimental values of the mean-free-path are given in Table 1.

III.F.3. The Experimental Set-Up For I-V Measurements.

Two techniques have been used in the measurement of the d.c. voltages across the SNS contact. The first, using conventional methods, was not adequate to accurately determine the first small voltages to appear across the contact. This method was used in early experiments and, later, to check the second method at higher voltages. The circuit is shown in Fig.20.

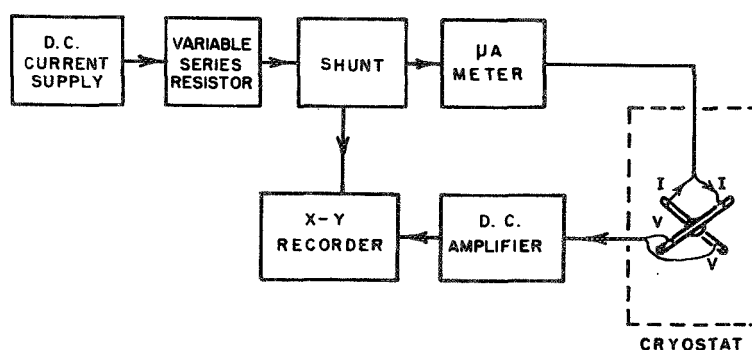


Fig.20 First Circuit Used to Determine I-V Characteristics.

The current source is a 0-6 v.d.c. filtered supply. The current from this is passed through a variable series resistance and on to a shunt. The shunt drives the y-axis of an x-y recorder. The current then passes through a uameter and on to the terminals of the sample. The voltage across the sample is detected with a Leeds and Northrup d.c. amplifier, whose output drives the x-axis of the x-y recorder.

As the construction of SNS junctions was improved, the normal resistance dropped to the order of a milliohm or less and junction voltages became very small for the small critical currents encountered. The techniques described above were limited by drift and thermal noise. The minimum detectable voltage changes were of the order of 100 nanovolts (nv). To circumvent the problem of noise and sensitivity, a phase-lock technique was developed.

For a phase-lock technique to work, the signal to be detected must be repetitive and fixed in frequency. In addition, there must be some reference phase for this signal. A lock-in amplifier (a narrow-band, tunable instrument that measures the in-phase component of the signal) is used to make the measurements.

To obtain the d.c. characteristics of the junction, a 4 kHz squarewave, switching between 0 and I , is used. When a voltage is developed across the junction, it switches from 0 to V . The lock-in amplifier measures the r.m.s. value of the principal Fourier component of the squarewave voltage. The output of the amplifier goes to an x-axis of a Hewlett-Packard x-y recorder. The recorder is calibrated, in d.c. nanovolts, with the lock-in amplifier's internal squarewave generator. This generator is also used to provide the current for the junction. Its output is amplified, passed through a variable resistance and a shunt and then on to the crossed wires (see Fig.21).

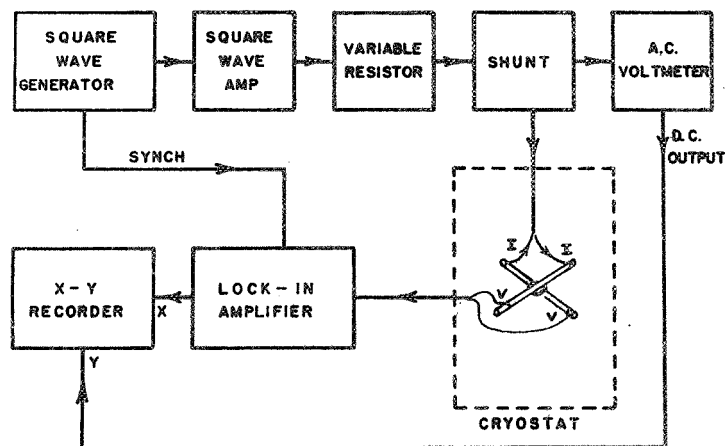


Fig.21 Experimental Set-Up For
Measuring the Junction I-V Characteristics.

An a.c. voltmeter (Hewlett-Packard, Model 400E) detects the voltage across the shunt. The amplified d.c. output is proportional to the d.c. current and drives the y-axis of the x-y recorder.

The lock-in amplifier is a Princeton Applied Research (PAR) Model HR-8. A type B1 preamplifier is used in the input. The input impedance of this unit is of the order of several ohms and most nearly matches the low impedance of the junction. With this combination, the noise voltage is of the order of $\frac{1}{2}$ nanovolt.

The voltage developed across the junction consists of a resistive and a reactive component. The latter is due to the inductance and capacitance of the associated circuit. By choosing the proper phase setting, one can measure just the resistive part of the signal, which is then amplified and converted to a d.c. signal in the lock-in amplifier.

To summarize this technique, a d.c. measurement is made on the junction by sending an interrupted d.c. current through it, detecting the resulting interrupted d.c. voltage that is generated, amplifying it and converting it into an uninterrupted d.c. signal.

III.F.4. The Experimental Set-Up For V-H Characteristics.

The magnetic properties of a Josephson junction are usually expressed in terms of the magnetic field vs the critical current. This procedure involves a tedious series of current-voltage measurements at various values of applied magnetic field. When one has obtained 50 or more I-V traces, the critical current can be measured and plotted vs H. The complete process can take several hours for a complete I_c vs H characteristic at a single temperature.

This technique has been replaced by a simple, less time consuming technique. For a fixed current, the voltage is plotted as a function of magnetic field. A second channel of the x-y recorder is used for this purpose. The circuit for doing this is shown in Fig.22. Here, the box labeled "current supply" (for the SNS junction) contains the generator, amplifier, resistance, shunt and voltmeter shown in Fig.21. I_H is the current that passes through the Helmholtz coil, producing the magnetic field. The shunt provides a voltage output which is proportional to I_H and, thus, H.

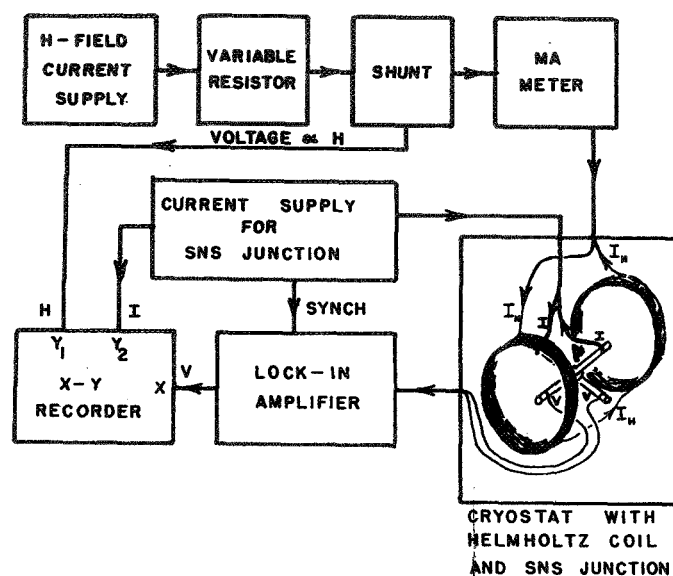


Fig.22 Experimental Set-Up For
Measuring the Junction V-H Characteristics.

III.F.5. The Experimental Set-Up For I-V Measurements
With A Second Current Introduced To The Junction.

A second current could be added to the junction by means of the gold film. The circuit for doing this is shown in Fig.23. The second current was fixed at some value, either positive or negative with respect to the junction current, and the I-V trace was obtained as described in Sec.III.F.3.

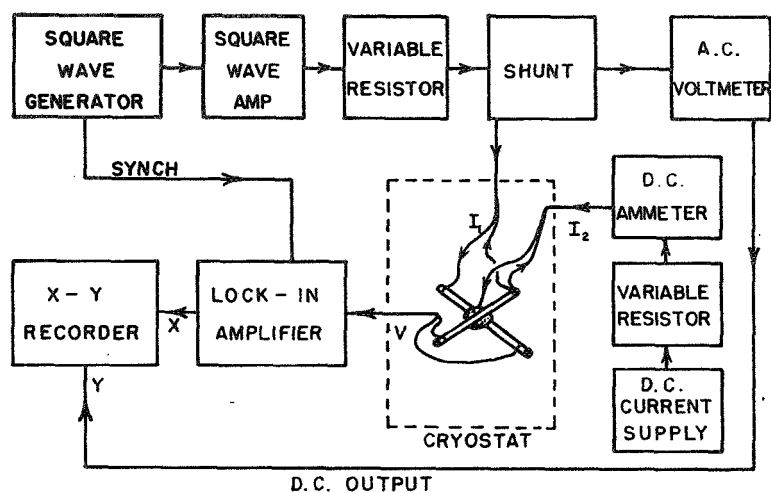


Fig.23 Experimental Set-Up For Measuring the I-V Characteristics, With a Second Current Applied To The Junction.

IV. Experimental Results.

IV.A. The Contact Area.

The tin wires used in this experiment had a diameter of 0.325 mm. When they were brought together under a force of approximately 50 grams (at right angles to one another), the load bearing area was approximately circular.

It should be noted that the contacts considered here are formed at 4.2K. At this temperature, the flow pressure*, P_f , of tin is 4.5×10^6 gm/cm². The load bearing contact area, πr^2 , is,

$$\pi r^2 = f/P_f \quad \text{IV.A.1}$$

where f is the contact force, and r is the effective radius of the contact.

As mentioned in Sec.III.A, previous experiments with contacts had indicated that the current carrying area of the junction was orders of magnitude less than the load bearing area. It was determined here that the load bearing area and the current bearing area are approximately the same. The technique used was to measure the period, ΔH , of the voltage oscillations on the V-H traces. Referring to Eqs.II.E.13 & 14, it will be seen that,

$$\Delta H = 2\pi / 2r(\delta_N + 2\lambda_L) \quad \text{IV.A.2}$$

*The flow pressure of gold-plated tin wires was determined experimentally. It was found that the addition of a 3000Å layer of gold increased the flow pressure, over that of bare tin, by approximately 10%.

This can be solved for r , and yields the area, πr^2 . Due to surface roughness and the fact that the contact is not necessarily circular, the area, calculated from this r is not exact. However, the results agree with load bearing areas calculated from Eq.IV.A.1. A comparison is made in Table 1.

Run	$\delta_N + 2\lambda$	ΔH	Load Bearing Area	Current Bearing Area
#	\AA	gauss	10^{-6}cm^2	10^{-6}cm^2
37	2720	1.36	10	100
38	2700	20.5	9.1	0.46
40	5200	0.67	3.4	110
41	8000	0.72	12.2	40.5
42	8300	0.80	11.2	30.2
43	5900	4.00	8.6	2.4
44	10,850	1.23	11.2	7.6
47	4700	1.34	18.1	34
48	11,300	0.92	6.8	12.4
49	11,300	1.23	15.0	7.0
50	8,500	0.93	15.5	21.8
51	8,500	1.23	14.0	12.4
52	12,500	0.77	14.0	15.1

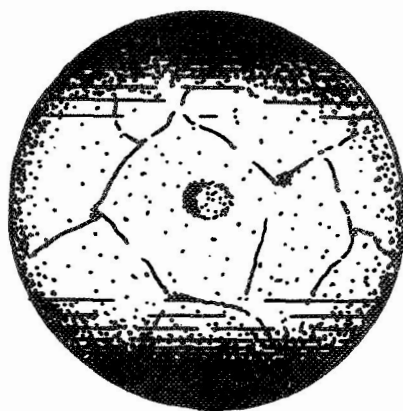
TABLE 1. LOAD BEARING AREA OF CONTACT
COMPARED WITH CURRENT BEARING AREA.

The worst agreement occurs when δ_N is very small. Then, surface roughness has its greatest effect on the cross-sectional area of the junction.

After the completion of an experiment, the contact area was observed, when possible, under a microscope. The measured area was generally found to be somewhat larger than the calculated load bearing area. It is felt that this discrepancy is due to two factors. First, a non-uniform load distribution (see, for example, Fig.11), over a small area, could cause the boundaries of the contact region to enclose a larger area than the load bearing area. Second, there may be a form of "surface tension effect" for small areas under stress. That is, the stress at a local area may deform a near-by region. This effect would be negligible for large areas (such as the ones used in experimentally determining the flow pressure), but might contribute to a larger observed depression for very small areas.

It is clear that one would not expect to see a smaller area than that calculated from the flow pressure. Fig.24 is a sketch of an observed contact area as seen under a microscope. Note the size of the individual grains.

It will be assumed in this experiment that the load-bearing area and the current-bearing area are the same unless the latter is self-field limited.



0.1mm

RUN NO. 42
 AREA = $15 \times 10^{-6} \text{ cm}^2$

Fig.24 A Sketch of a Contact
 Region as Seen Under a Microscope.

IV.B. The Critical Current Density.

The critical current is defined as that current through the junction for which a voltage first appears across the junction. It is temperature dependent and, near T_c , difficult to determine. Fluctuations are the major source of difficulty, as they round the I - V traces.

It was experimentally determined that I_m is not accurately found by nulling the earth's magnetic field before the experiment and leaving it unchanged. There

appears to be a temperature dependent field at the contact which must be nulled for every separate I-V trace. The effect is especially noticable for contacts with thin normal metal layers and high critical currents, and is probably caused by the self-field of the junction currents coupled with a large temperature dependence of the penetration depth near T_c .

The experimental procedure is to set the current at a value greater than I_m and then vary H_x and H_y to obtain a minimum voltage. After this, an I-V trace is taken. Below 3K, the procedure becomes unnecessary, except for high critical currents. Fig.25 illustrates an example of an I_m vs T trace, taken before this phenomena

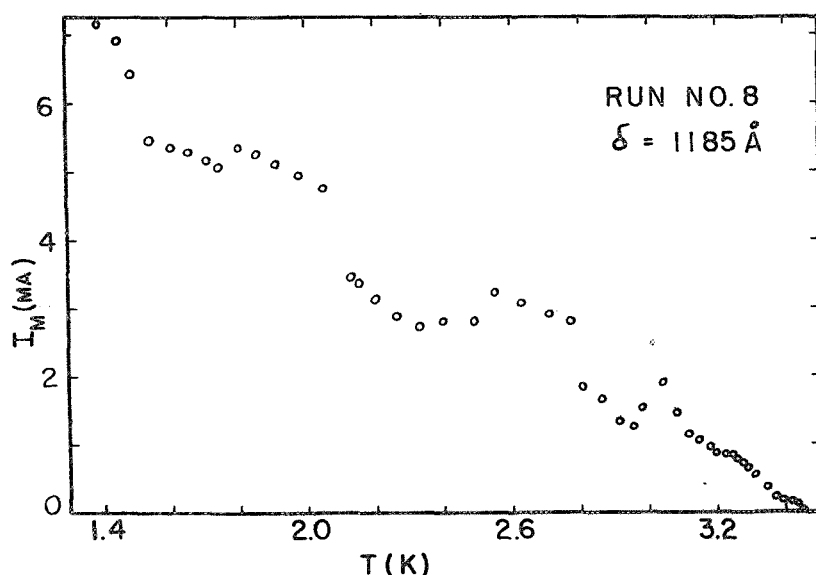


Fig.25 I_m vs T With no Corrections
Made in the Applied Magnetic Field.

was noticed. Fig.26 shows a trace of I_m vs T with the applied field optimized for maximum I_m .

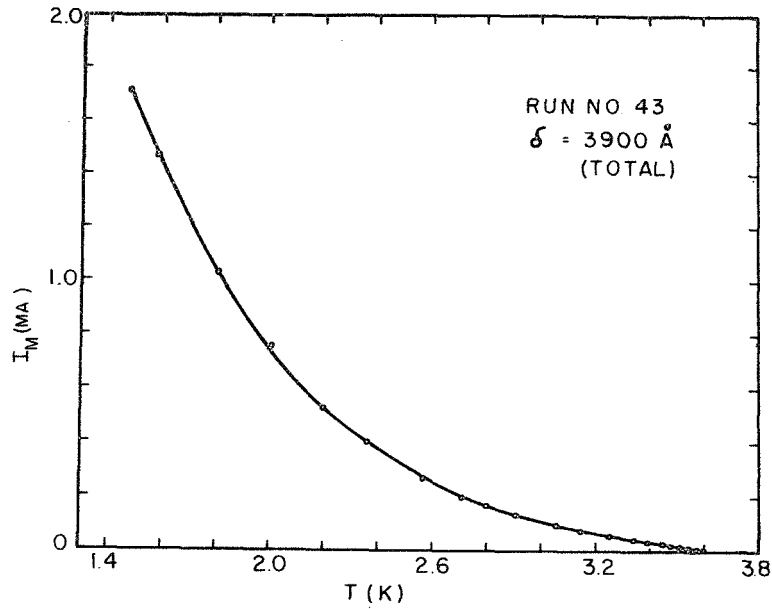


Fig.26 I_m vs T With the Applied Magnetic Field Optimized for I_m .

The changes necessary in the applied field were generally of the order of 0.05 gauss.

The critical current density, j_m , will be defined as the critical current divided by the load-bearing area and will given in units of amperes/cm². From the simple model used in Sec.II.C., it is seen that the magnitude of j_m varies as $\exp(-\delta_N/\xi_N)$, for a fixed temperature. A plot

of the logarithm of the critical current density versus the total normal metal thickness should give a straight line, if ξ is reasonably constant. Fig.27 is such a plot, obtained from data taken at 2K. Included in the data are some results obtained by Meissner⁴³ for gold-plated tin wire contacts. Note that $j_c = j_m$ in the absence of a magnetic field.

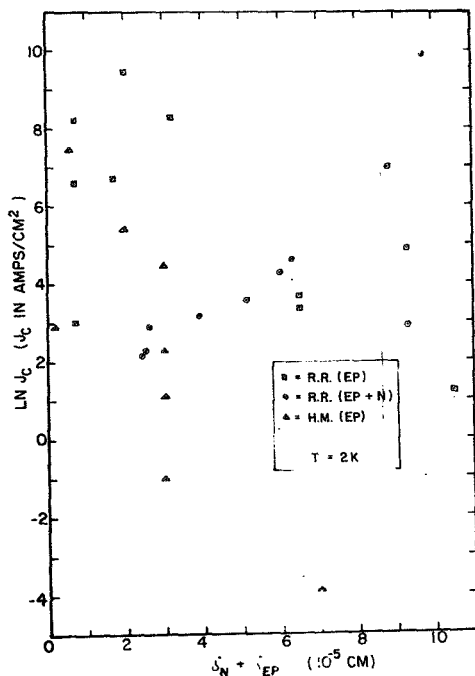


Fig.27 $\ln j_c$ vs $\delta_N + \delta_{EP}$

As can be seen from these results, the simple model used in Sec.II.C is not sufficient to explain the data.

It is felt that the rather high contact resistance, encountered in these junctions, plays a major role in

determining the critical current. A decrease in resistance is found when the tin wires are electroplated with up to 500⁰A of gold. Thereafter, no correlation between gold thickness and resistance can be found. Also, measurements of the resistivity of gold films at 4.2K (less than 10^{-6} ohm-cm) lead to an expected contact resistance of less than 10^{-4} ohms. This is a maximum figure, taking into account the channel resistance of the contact⁵⁵.

The results of 20 experiments, performed before the gold-plating technique was developed, showed that, when the resistance was more than 10×10^{-3} ohms, the SNS contact did not become measurably superconducting. To explain the data obtained, a model is proposed, based on the assumption that a thin boundary layer of high disorder and short mean-free-path exists between the tin wire and the gold. It is proposed that this layer (to be called the "M" layer) is completely responsible for the anomalous contact resistance. Physically, it is probably composed of gold, tin oxide and intermetallic compounds. It will be assumed that the properties of this layer are constant for all experiments. Only the thickness of this layer may vary.

55. R. Holm, Electric Contacts (Hugo Gebers Forlag, Stockholm, 1946), p.16.

The new model to be used is represented in Fig.28.

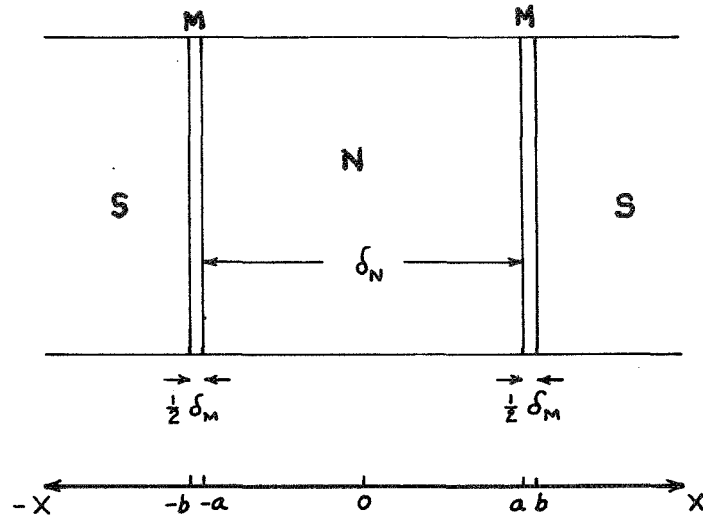


Fig.28 A Model of the SNS Contact, Including the M Layer.

δ_N is the total thickness of the M layers. Fig.29 shows

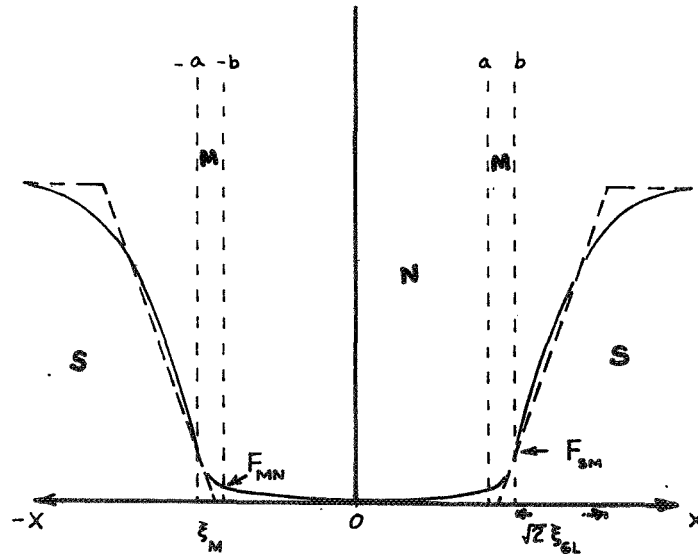


Fig.29 Model of the SNS Contact Showing the Condensation Amplitude.

the model used to calculate the condensation amplitude, F , at the boundaries. The dotted line represents the straight line approximation to the boundary value, F_{SM} , of F at the superconductor-M layer interface. The unbroken line represents the shape of $F(x)$. Repeating the analysis used in Secs. II.B & C, assuming that F is continuous across the MN boundary, and assuming that F has the same dependence in M as in a normal metal, it is found that,

$$F_{EP}(x) = (\xi_M / \sqrt{2} \xi_{\epsilon}) |F_S(\infty)| \exp(\frac{1}{2} \phi_M / \xi_M) \left\{ \exp[-(x + a)/\xi_{EP} + i\theta_{-b}] + \exp[(x - a)/\xi_{EP} + i\theta_b] \right\}$$

IV.B.1

where ξ_{EP} is the coherence length in the electroplated gold, given by,

$$\xi_{EP} = [h v_{ep} \ell_{ep} / 6\pi kT]^{\frac{1}{2}} \quad (\text{dirty limit}) \quad \text{IV.B.2}$$

v and ℓ are the Fermi velocity and mean-free-path, and ξ_M is the coherence length in the M layer, given by,

$$\xi_M = [h v_m \ell_m / 6\pi kT]^{\frac{1}{2}} \quad \text{IV.B.3}$$

Applying Eq.II.C.4, the critical current density is found to be,

$$j_c = \frac{2v_s^2 \ell_s^2 e \hbar |F_S(\infty)|^2 \xi_M}{v_m^2 \ell_m^2 m \xi_{GL}^2} \exp[-(\delta_{EP} / \xi_{EP} + \delta_M / \xi_M)]$$

IV.B.4

where $\rho_M \delta_M$ can be found from the normal resistance of the contact by,

$$R_N = \rho_M \delta_M / \pi r^2 \quad \text{IV.B.5}$$

and where ρ_M is the resistivity (unknown) of the M layer. Then the $\ln j_c$ is,

$$\ln j_c = a_1 - \delta_{EP} / \xi_{EP} - R_N \pi r^2 / \rho_M \xi_M \quad \text{IV.B.6}$$

where,

$$a_1 = \ln \left[\frac{2v_s^2 \ell_s^2 e \hbar |F_S(\infty)|^2 \xi_M}{v_m^2 \ell_m^2 m \xi_{GL}^2} \right] \quad \text{IV.B.7}$$

This expression illustrates the dependence of $\ln j_c$

on the gold thickness, contact area and contact resistance.
 ξ_{EP} and $\rho_M \xi_M$ must be found experimentally.

Following the analysis of Sec.II.C., the temperature dependence of the critical current density is given by,

$$\ln j_c = C'_0 + f(t) - C'_I t^{\frac{1}{2}} \quad \text{IV.B.8}$$

with the temperature independent constants given by,

$$C'_0 = \ln \left[\frac{2v_s^2 \ell_s^2 e \hbar (\hbar v_m \ell_m)^{\frac{1}{2}} [\Delta(0)]^2}{m v_m^2 \ell_m^2 V^2 (6\pi k T_c)^{\frac{1}{2}} (0.55 \xi_0^2)} \right] \quad \text{IV.B.9}$$

and,

$$C'_I = [6\pi k T_c / \hbar]^{\frac{1}{2}} [\xi_{EP} / (v_{EP} \ell_{EP})^{\frac{1}{2}} + R_N \pi r^2 / \rho_M (v_m \ell_m)^{\frac{1}{2}}] \quad \text{IV.B.10}$$

and where $f(t)$ is given by Eq.II.C.10 and plotted, vs t , in Fig.4. This temperature dependence is for gold in the dirty limit and tin in the clean limit. The latter only involves the value of C'_0 .

In the case where a single crystal gold film has been

sandwiched between the gold-plated tin wires, the new model must be extended. This is shown in Fig.30.

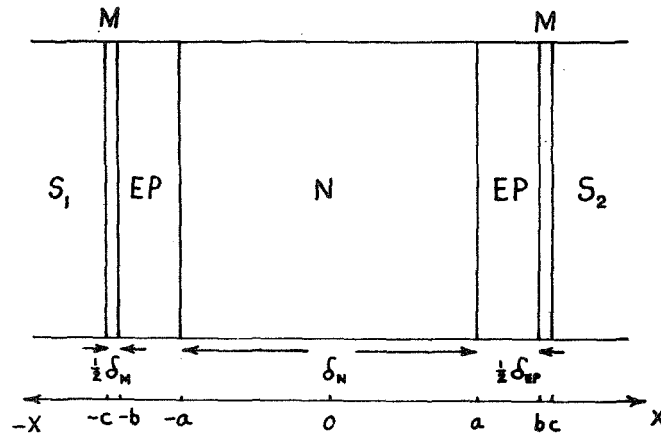


Fig.30 A Model of the SNS Contact Including the M Layer, Gold-Plating and a Single Crystal Gold Film.

The single crystal gold film is represented by "N", and it has a thickness of δ_N .

It will be assumed that there is a negligible barrier between the gold film and the gold-plating, and that $F(x)$ is continuous across the boundary. Then, following the same analysis as before, the critical current density is given by,

$$\ln j_c = a_1 - \delta_{EP} / \xi_{EP} - \delta_N / \xi_N - R_N \pi r^2 / e_M \xi_M$$

IV.B.11

with a_1 given by Eq.IV.B.7, and where ξ_N can be obtained from a measurement of the mean-free-path in the gold film.

The temperature dependence of the critical current density, in the dirty limit, is,

$$\ln j_c(t) = C'_0 + f(t) - C''_I t^{\frac{1}{2}} \quad \text{IV.B.12}$$

with C'_0 given by Eq.IV.B.9, $f(t)$ given by Eq.II.C.10 and with C''_I given by,

$$C''_I = [6\pi kT_c / \hbar]^{\frac{1}{2}} \times \\ [\delta_{EP} / (v_{ep} l_{ep})^{\frac{1}{2}} + \delta_N / (v_N l_N)^{\frac{1}{2}} + R_N \pi r^2 / e_M (v_m l_m)^{\frac{1}{2}}]$$

IV.B.13

If the single crystal gold film is in the clean limit, the temperature dependence is given by,

$$\ln j_c(t) = C_0' + f(t) - C_I' t^{\frac{1}{2}} - C_{II}' t \quad \text{IV.B.14}$$

with C_I' given by Eq.IV.B.10 and C_{II}' given by,

$$C_{II}' = [2\pi k T_c / \hbar v_N] \delta_N \quad \text{IV.B.15}$$

If Eq. IV.B.6 is correct, the temperature dependent parameters ξ_{EP} and $\rho_M \xi_M$ can be evaluated from the data of those experiments where there was no single crystal gold film. The data at 2.00K (where fluctuations have a negligible effect) will be used.

The method is to plot $\ln j_c$ versus $\delta_{EP} + [\xi_{EP} / \rho_M \xi_M] R_N \pi r^2$. If a straight line is obtained, the slope will be $-1/\xi_{EP}$. It will be assumed that ξ_{EP} is the same for all experiments so that $[\xi_{EP} / \rho_M \xi_M]$ is also constant. This ratio is not known, but can be found by trial and error. The data is plotted for various values of $[\xi_{EP} / \rho_M \xi_M]$ and the value that most nearly gives a straight line is chosen. This has been done, and the result is shown in Fig. 31.

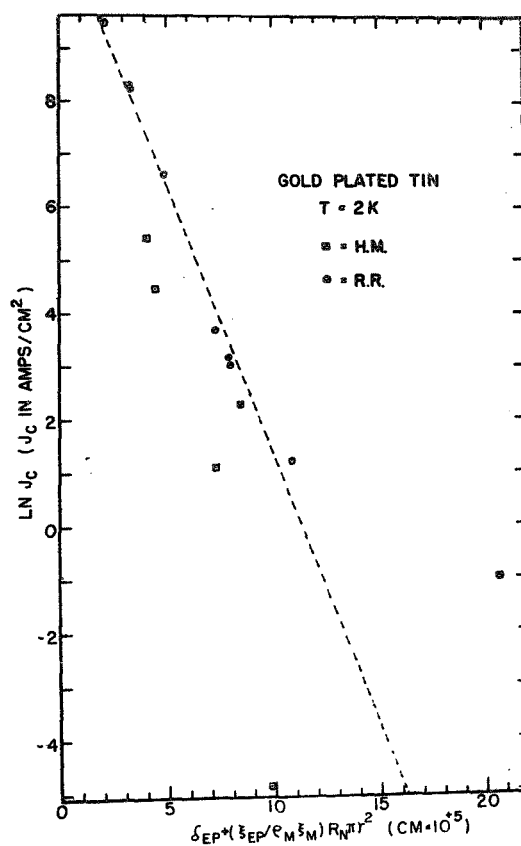


Fig.31

$$\ln j_c \text{ vs } \delta_{EP} + [\xi_{EP} / e_M \xi_M] R_N \pi r^2$$

The value of $[\xi_{EP} / e_M \xi_M]$ is $1200 \text{ ohm}^{-1} \text{cm}^{-1}$ for this plot. The slope of the line gives a value for ξ_{EP} of 890 \AA . Then $e_M \xi_M$ is found to be $7.4 \times 10^{-9} \text{ ohm-cm}^2$.

Included with this data are data from the initial

results of Meissner⁴³. This data was not taken with the benefit of optimum magnetic field settings, and thus the j_c obtained would tend to be on the low side.

Now Eq.IV.B.11 can be checked by plotting the data from the experiments where a single crystal gold film was used. If $\ln j_c$ is plotted vs $\delta_{EP} + \delta_N \xi_{EP} / \xi_N + [\xi_{EP} / e_M \xi_M] R_N \pi r^2$. ξ_N is found by applying Eq.II.B.5 (in the dirty limit). This has been done in Fig.32.

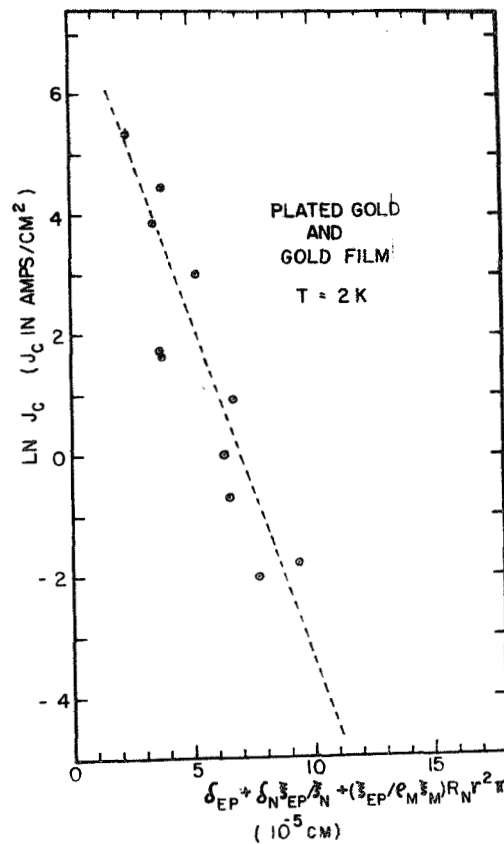


Fig. 32

$$\ln j_c \text{ vs } \delta_{EP} + \delta_N \xi_{EP} / \xi_N + [\xi_{EP} / e_M \xi_M] R_N \pi r^2$$

The dashed line has a slope $(-1/\xi_{EP})$ corresponding to $\xi_{EP} = 890\text{\AA}$ and this seems to fit the data quite well.

No attempt has been made to evaluate the intercept on the $\ln j_c$ axis (where the normal metal thickness, contact area and resistance approach zero) because of the number of parameters that enter into the evaluation of a_1 . However, it would appear that the gold-plated tin contacts exhibit a larger value for the intercept than do the contacts with a gold film. This is probably due to an additional boundary layer (a monolayer of adsorbed gas on the surface of the gold) and discontinuity introduced by the additional gold film.

The temperature dependence of the critical current density (Eqs. IV.B.8, 12 & 14) can be checked by plotting $\ln j_c - f(t)$ vs $t^{\frac{1}{2}}$ in the dirty limit. For low temperatures, $f(t)$ does not vary greatly and $\ln j_c$ vs $t^{\frac{1}{2}}$ should approach a straight line. This has been done in Fig. 33, where only data points corresponding to a current density of $\ln j_c = 1$, or greater, have been shown. In these plots, j_c is expressed in amperes/cm².

Clarke²⁴ has made a similar plot for the data obtained for vapor-deposited thin film Josephson junctions

(SNS), and the results are similiar.

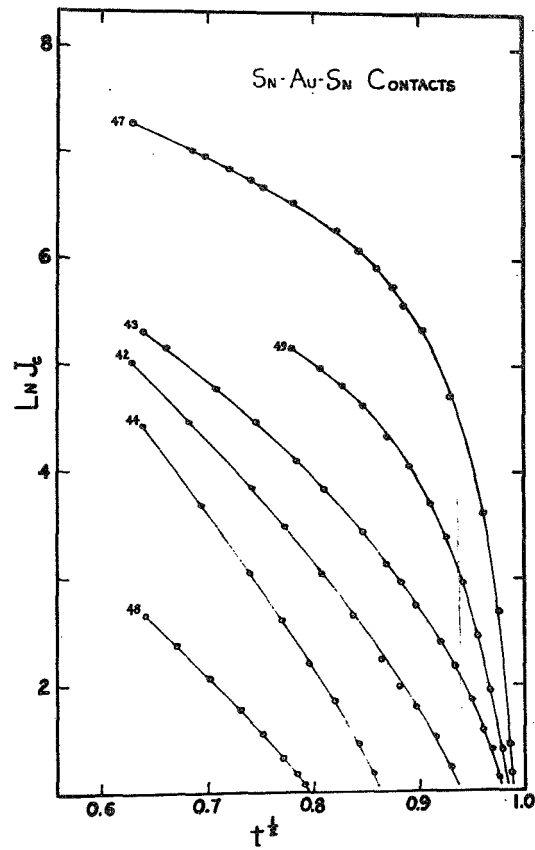


Fig.33 $\ln j_c(t)$ vs $t^{\frac{1}{2}}$

To show the complete temperature dependence, the constants C_I' , C_I'' , and C_{II} must be evaluated. C_I' is found to be, at 2.0K,

$$C_I' = 1.51 \times 10^5 \delta_{EP} + 1.82 \times 10^7 R_N \pi r^2 \quad \text{IV.B.16}$$

where δ_{EP} is in cm, R_N is in ohms and πr^2 is in cm^2 . To obtain this value, the value of ℓ_{EP} @ 2.0K had to be determined from Eq.IV.B.2, with $\xi_{EP} = 8.90 \times 10^{-6} \text{cm}$. This was, $\ell_{EP} = 276 \times 10^{-8} \text{cm}$. C_I'' is found to be,

$$C_I'' = 1.51 \times 10^5 \delta_{EP} + 2.51 \times 10^2 \delta_N / (\ell_N)^{\frac{1}{2}} + 1.87 \times 10^7 R_N \pi r^2 \quad \text{IV.B.17}$$

and C_{II} is found to be,

$$C_{II} = 2.1 \times 10^4 \delta_N \quad \text{IV.B.18}$$

where lengths are in cm and resistance in ohms.

In Fig. 34, the complete temperature dependence is checked by plotting $\ln j_c - f(t)$ vs $t^{\frac{1}{2}}$. For the dirty limit, the data should give a straight line with a slope of $-C_I'$. On the figure, the expected slope has been drawn in as a dashed line. The agreement is good except for the case of very high current densities. It is felt that, in those circumstances, the junction is in the region of self-field limiting. That is, for high critical currents, the supercurrent is limited to an area around the edge of the junction, and the actual current density is considerably greater than that calculated from the load area. It would be expected that, for

decreasing temperatures, the measured current density would fall below the expected current density.

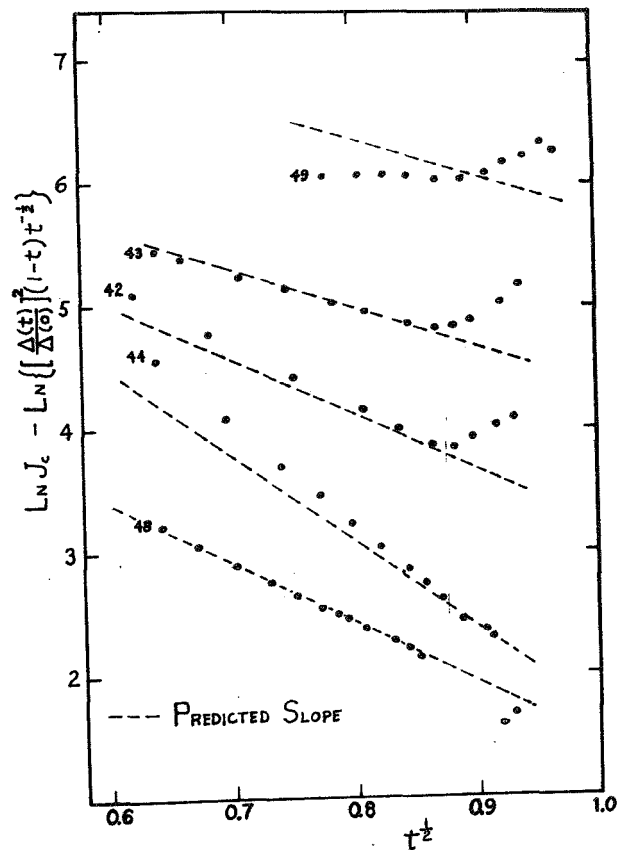


Fig.34 $\ln j_c - f(t)$ vs $t^{\frac{1}{2}}$

It can be seen that the data seems to fit the equations governed by the dirty limit. For a gold film at 2K, with a mean-free-path of $20,000\text{\AA}$, ξ_N , calculated in the dirty limit, is $2,380\text{\AA}$, while in the clean

limit, it is $8,560\text{\AA}$. Apparently, a much longer mean-free path is necessary to be in the clean limit.

It should be noted that the term, $\ln j_c - f(t)$, is the difference between two logarithmic terms. Very near T_c , $f(t)$ varies rapidly with t . In this region, there is a very high possibility of error, which could explain the anomalous behavior of $\ln j_c - f(t)$ near $t = 1$ on Fig.34.

In conclusion, the behavior of the Josephson critical current density, as a function of contact resistance, contact area, normal metal thickness and temperature seems to be well explained by the extended model developed in this section. The following tables, 2, 3, and 4 provide a summary of the data used in this analysis.

TABLE 2. DATA FOR ELECTROPLATED SNS CONTACTS.

Run	δ_{EP}	R_N	πr^2	$\frac{\sum_{EP} R_N \pi r^2}{C_m \sum_m}$	$\delta_{EP} + \frac{\sum_{EP} R_N \pi r^2}{C_m \sum_m}$	$I_c @ 2K$	$\ln j_c @ 2K$	C_I'
#	10^{-8} cm	$10^{-3} \Omega$	10^{-6} cm^2	10^{-8} cm	10^{-8} cm	10^{-6} amp	$j_c \text{ in a/cm}^2$	-
21	2,000	0.153	10.6	195	2,195	145×10^3	9.44	3.03
35	700	4.40	5.0	2,640	3,340	18.8×10^3	8.23	1.45
37	720	6.00	10.0	7,200	7,920	200	3.0	2.16
38	700	3.75	9.1	4,100	4,800	6,730	6.6	1.67
40	3,200	0.306	3.4	125	3,325	13,500	8.28	4.82
47	1,700	0.149	18.1	325	2,025	14,700	6.70	2.60
50	6,500	0.380	15.5	710	7,210	605	3.68	9.86
51	6,500	0.770	14.0	1,300	7,800	400	3.35	9.95
52	10,500	0.214	14.0	360	10,860	46	1.2	15.8

TABLE 3. DATA FOR ELECTROPLATED SNS CONTACTS WITH GOLD FILM

Run	δ_N	δ_{EP}	R_N	πr^2	$\delta_{EP} + \frac{\delta_N \delta_{EP}}{3N} + \frac{3EP R_N \pi r^2}{C_m \delta_m}$	λ_N	$\ln j_c @ 2K$	C_I''
#	10^{-8} cm	10^{-8} cm	$10^{-3} \Omega$	10^{-6} cm^2	10^{-8} cm	10^{-8} cm	$j_c \text{ in a/cm}^2$	-
31	1590	1000	4.00	17	9330	90,000	-1.8	2.89
33	1680	700	3.70	12.8	6570	65,000	0.9	2.13
34	1680	800	0.77	60	6520	65,000	0	2.25
39	4500	650	3.10	15.2	7540	3,700	-2.0	3.55
41	4500	1500	0.637	12.2	3680	3,700	1.8	4.25
42	4500	1800	0.213	11.2	3300	3,700	3.86	4.61
43	2200	1700	1.80	8.6	3800	23,000	4.44	3.16
44	5000	3850	0.440	11.2	5175	13,000	3.01	6.98
45	4500	5250	0.630	12.0	6400	3,700	-0.70	9.88
48	7500	1800	0.403	6.8	3550	7,800	1.66	4.88
49	8300	1000	0.226	15.0	2420	19,000	5.35	2.90

TABLE 4. DATA FOR ELECTROPLATED TIN CONTACTS (Sn - Au - Sn) - H. Meissner

Run	δ_{EP}	R_N	πr^2	$\frac{\delta_{EP} R_N \pi r^2}{\rho_m \xi_m}$	$\delta_{EP} + \frac{\delta_{EP} R_N \pi r^2}{\rho_m \xi_m}$	$\ln j_c @ 2K$
#	10^{-8} cm	$10^{-3} \Omega$	10^{-6} cm ²	10^{-8} cm	10^{-8} cm	j_c in a/cm ²
Au 1	200	592	13.3	943,000	943,000	2.89
Au 2	600	12.5	13.3	19,900	20,500	7.45
Au 3	2,000	1.26	13.3	2,000	4,000	5.41
Au 4	3,000	11.1	13.3	17,700	20,700	-0.99
Au 5	3,000	1.01	11.3	1,370	4,370	4.44
Au 6	3,000	0.27	136	4,420	7,420	1.08
Au 7	3,000	0.22	206	5,450	8,450	2.27
Au 8	7,000	1.75	13.3	2,800	9,800	-4.89 est/
Au 9	22,000	5.9	13.3	9,450	31,450	0

IV.C. Transition Curves.

The transition from the normal to the superconducting state is characterized by the corresponding resistance vs temperature plot. This has been found to exhibit a strong dependence on the contact current, as illustrated in Fig.35 for two representative contacts.

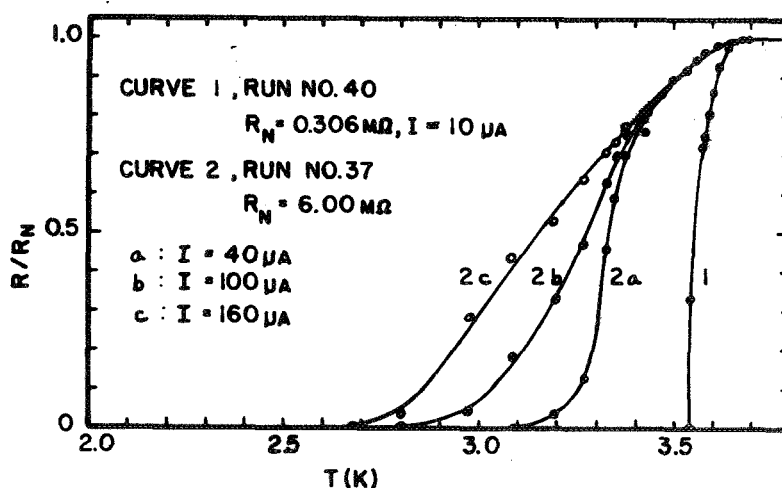


Fig.35

Reduced Contact Resistance vs Temperature.

A qualitative explanation for this dependence can be found if one assumes that the current vs voltage characteristics of the junction are the same as those expressed by Eq.II.E.8. If the temperature dependence of j_c (as in Eq.IV.B.12) is added to Eq.II.E.8, it is found that,

$$R(t)/R_N = [1 - (1 - t)^4/\kappa^2] \quad \text{IV.C.1}$$

for temperatures near T_c . κ is a dimensionless constant, proportional to the fixed current used in the measurement of R . This expression is plotted in Fig.36, for different values of κ .

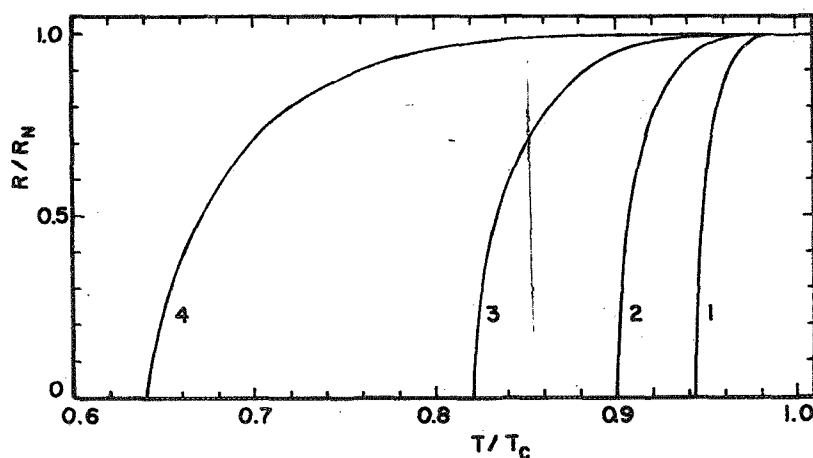


Fig.36 An Ideal Plot of
Reduced Resistance vs Temperature.

In an actual experiment with tin contacts, the reduced temperature must be referenced to the transition temperature of tin, under the pressure of the contact. For a flow pressure of tin equal to $4.5 \times 10^6 \text{ gm/cm}^2$, the decrease in T_c is approximately 0.18K, resulting in a T_c

of 3.54K ⁵⁶. However, if the tin is under this pressure, only in the vicinity of the contact, one would expect that, in the temperature range of 3.54K to 3.72K , some tunneling could take place across the remaining normal region. This would result in a continuous decrease in contact resistance as the temperature was lowered below 3.72K .

Another effect that enters into the shape of the R/R_N vs t characteristics is that of fluctuations. They are characterized by the parameter γ , which approaches zero as the effect becomes worse (see Fig.9 and Eq.II.E.11). As the temperature of the contact is lowered, the critical current increases. Since γ is directly proportional to the critical current, the effect of fluctuations will decrease with temperature. The result of this, on the R/R_N vs t characteristics is shown in Fig.37. Curve 1 is a reproduction of curve 1 of Fig.36, not including the effect of fluctuations. Curve 2 is for the same case, but including the effect of fluctuations. A noise temperature of 48K has been arbitrarily chosen. Curve 3 is for the same noise temperature and a higher value of the fixed current used to measure R . The curves have been

56. Nils L. Muench, Phys. Rev. 99, 1814 (1955).

obtained by using Eq.IV.C.1 along with Fig.9 to find R/R_N .

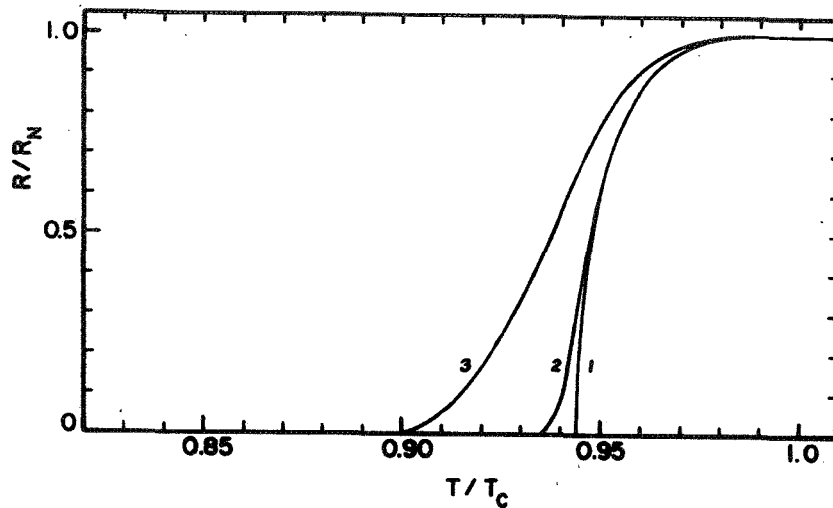


Fig.37 An Ideal Plot of Reduced Resistance vs Temperature, Taking Into Account the Effect of Fluctuations.

In conclusion, it is felt that a combination of Eq.II.E.8 and fluctuation theory is capable of giving an explanation of the R/R_N vs t curves obtained by experiment. A detailed calculation has not been attempted.

IV.D. Current-Voltage Characteristics of the Contact.

The current-voltage characteristics of the SNS contact, as expressed in Eq.II.E.8, have been obtained experimentally. A comparison between the theory and the data is made in Figs.38, 39 and 40, for a typical contact. The I-V characteristic, predicted by Eq.II.E.8, has been plotted as a dashed line. A contact resistance, R_N , of 0.309×10^{-3} ohms was used for this temperature.

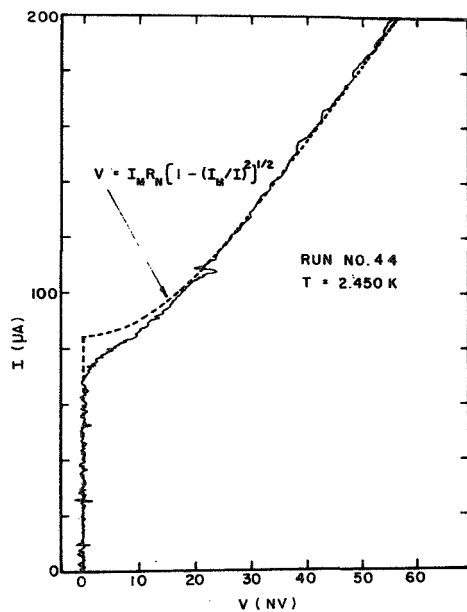


Fig.38 I-V Plot
@ T = 2.45K, Run # 44.

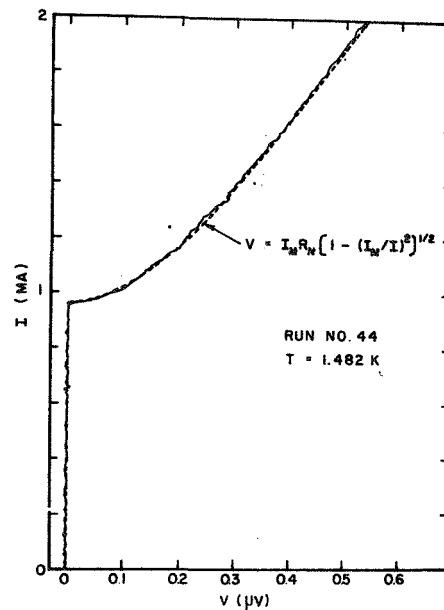


Fig.39 I-V Plot
@ T = 1.48K, Run # 44.

The rounding of the I-V curve in Fig.38 is due to fluctuations, and corresponds to a γ of about 100.

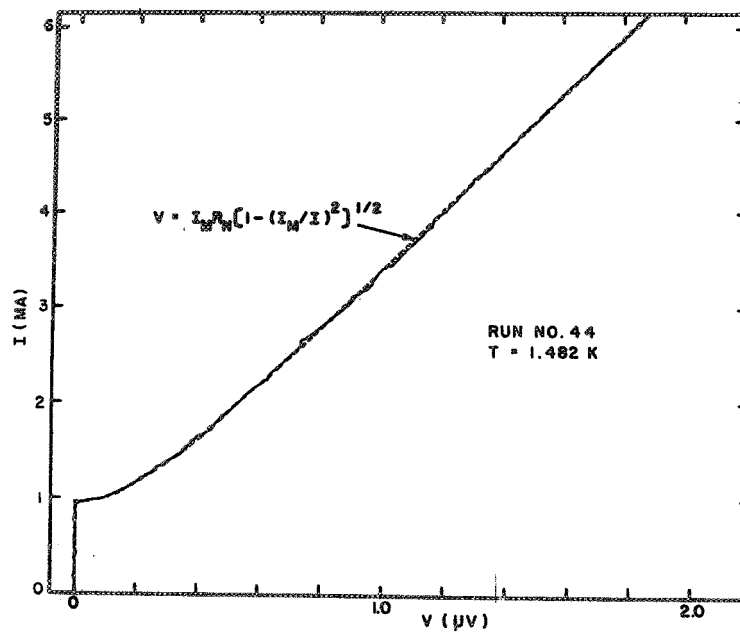


Fig.40 I-V Plot, @ $T = 1.48K$, Run# 44.

Fig.41 shows the effect of severe fluctuations on an I-V characteristic. From Eq.II.E.11, the numerical value of γ is,

$$\gamma = 4.75 \times 10^7 I_C / T_{\text{noise}} \quad \text{IV.D.1}$$

where I_C is expressed in amperes, and T in degrees Kelvin.

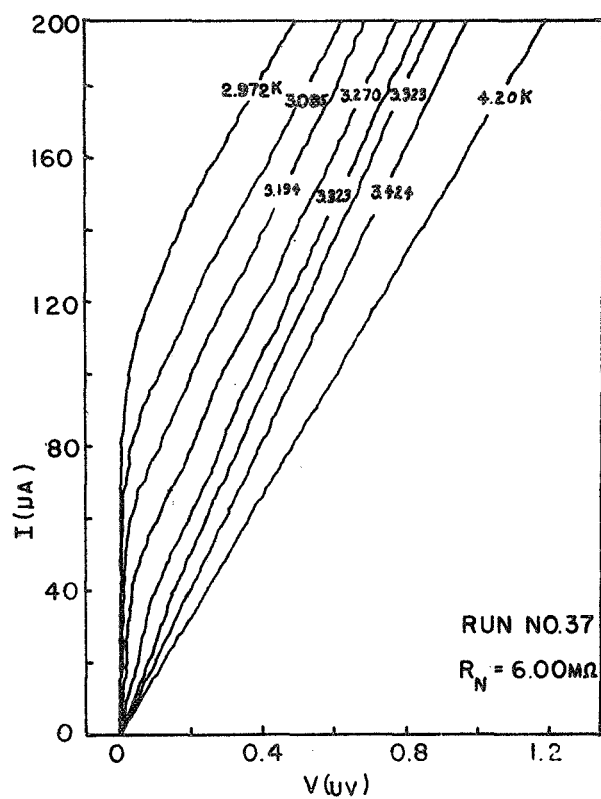


Fig.41 I - V Plots at
Different Temperatures, Run # 37.

As the contact temperature is lowered, I_c increases, thus increasing γ . This data should be compared with Fig.9. The effective noise temperature for this run is of the order of 80K.

IV.E. The Voltage-Magnetic Field Characteristics.

The magnetic field applied to the SNS junction alters the junction voltage, as explained in Sec.II.E.4. The V-H characteristics are especially important because they illustrate the unique, periodic behavior, characteristic of the Josephson junction. They have been used, in Sec.IV.A., to confirm the current carrying area of the contact as being the same as the load bearing area. In addition, they shall be shown to exhibit direct proof for the existence of supercurrents in the junction, when the critical current has been exceeded.

Fig.42 reproduces the V-H characteristics, at two temperatures, for Run # 41. The current has been fixed at

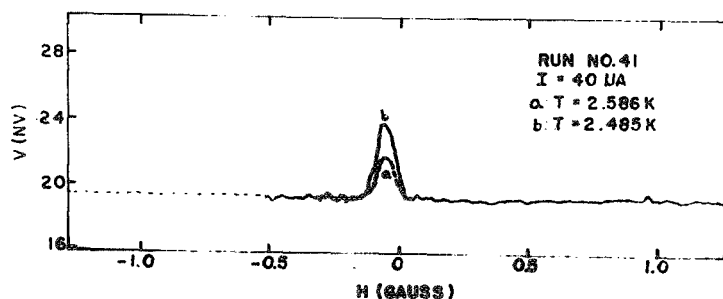


Fig.42 V - H Plots, Run # 41.

a small value, and the voltage has been recorded as the magnetic field was varied from -1 gauss to $+1$ gauss. An unexplained effect is noticed here. There is a maximum in the voltage at $H = 0$ (It must be assumed that there was a stray field of about 0.07 gauss present here). As the temperature was lowered, this peak in the voltage was replaced by a minimum. This is shown in Fig.43.

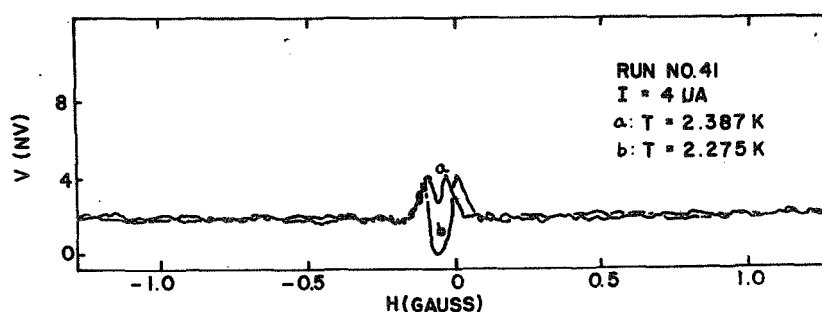


Fig.43 V-H Plots, Run # 41.

Figs.44 and 45 show the V-H characteristics for another junction. The phenomena mentioned for Run # 41 was not noticed here. There is a noticeable discontinuity in V seen in Fig.44. This is believed to be due to the critical field of tin.

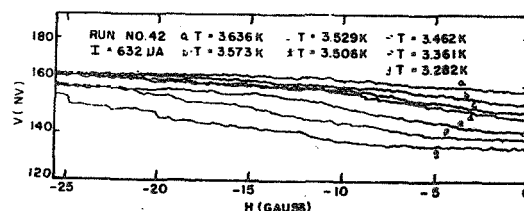


Fig.44 V-H Plots, Run # 42.

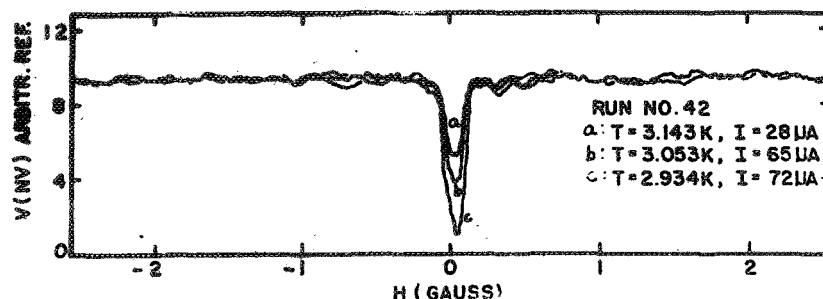


Fig.45 V-H Plots, Run # 42.

It is felt that, for temperatures near T_c , the smooth increase in voltage, as H is increased, is due to the suppression of superconductivity in the tin in the immediate vicinity of the contact. At these temperatures, there seems to be no evidence of a Josephson current. However, it is entirely possible that a supercurrent exists which is too small to detect.

The discontinuity in the V-H plots, mentioned above, has been plotted as a function of T . Fig.46 is a plot of H_D vs T for Run # 38. H_D is the magnetic field value for which the discontinuity occurs. The temperature dependence exhibited here is similar to that of the bulk critical field of a superconductor. A plot of H_D vs T^2 yields a straight line. However, the extrapolated value of H_D , at $T = 0$, is approximately $\frac{1}{4}$ that of the critical bulk field value. This is undoubtedly due to the increase of H in

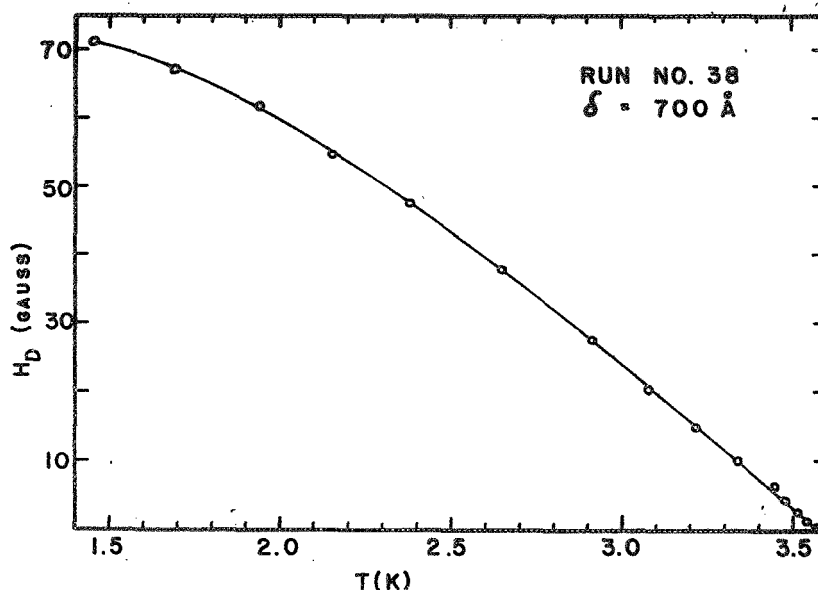


Fig.46 H_D vs T .

the neighborhood of a superconductor (a result of the Meissner effect). For an infinite cylindrical superconductor in a transverse field, the field at the surface of the superconductor should be twice the applied field⁵⁷. With the crossed wire geometry used here, it is quite probable that the field at the junction is three to four times the applied field. Fig.47 is a reproduction of some of the data from which Fig.46 was obtained. As the temperature is lowered, H_D increases and more of the Josephson interference pattern becomes apparent. The value of H_D is

57. E.A. Lynton, see ref.15, p.25.

found to be independent of the current through the contact.

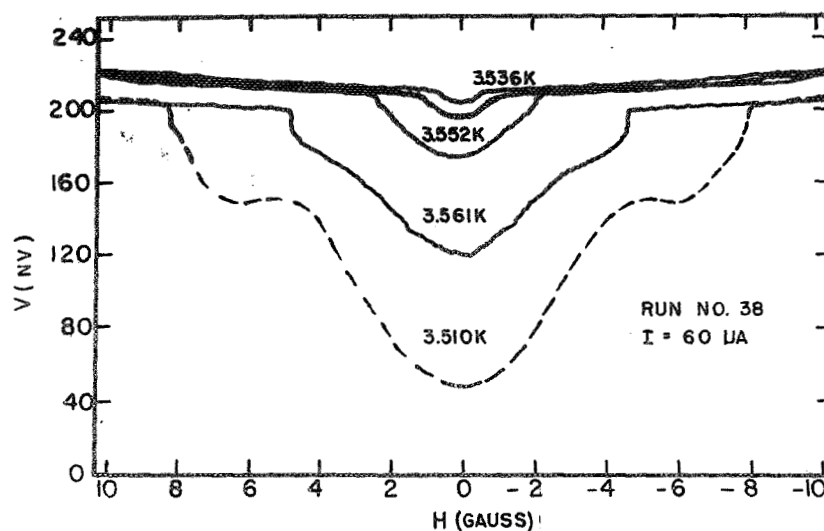


Fig.47 V - H Plots, Run # 38.

The behavior of the V-H characteristics at lower temperatures is shown in Figs.48 and 49. The sharp dip in the characteristic is typical. In Fig.48, this dip is shown on an expanded scale as well. Fig.49 shows the discontinuity in V.

If Josephson tunneling ceased, when the critical current of the junction were exceeded, there would be no oscillations of the voltage observed in the V-H characteristics. However, with the excess supercurrents predicted by Stewart³⁸, one would expect to see such oscillations.

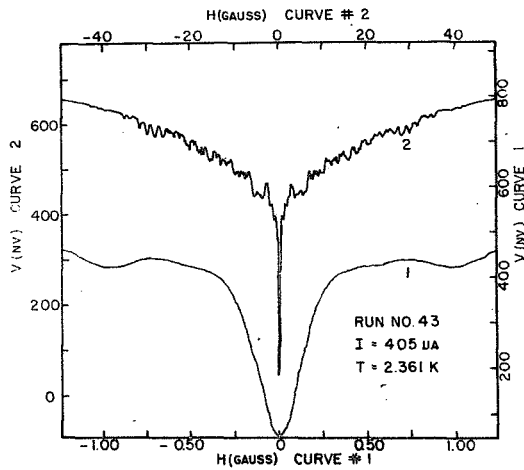


Fig.48 V-H Plots,
Run # 43.

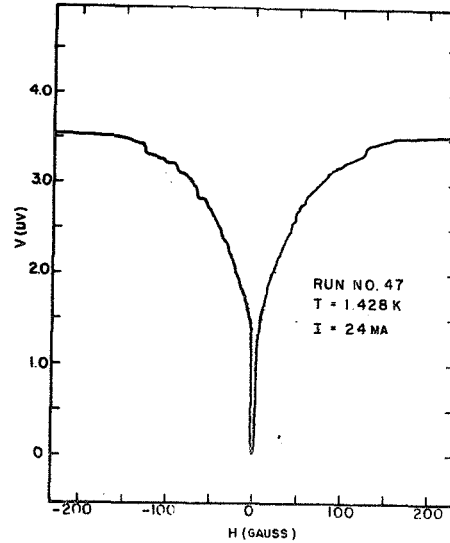


Fig.49 V-H Plots,
Run # 47.

The magnitude of the voltage oscillation, ΔV , is given by,

$$\Delta V = IR_N - V \quad \text{IV.D.2}$$

with V given by Eq.II.E.8. ΔV is measured between the first and second minimums in the voltage on a V-H characteristic. It can be rewritten as,

$$\Delta V = I R_N [1 - (1 - I_m^2 / I^2)^{\frac{1}{2}}] \quad \text{IV.D.3}$$

These oscillations have been observed for currents well in excess of I_m . Fig.50 shows a plot of ΔV vs I for Run # 40. The temperature was fixed at 3.459K and the current was varied up to 7 times the critical current.

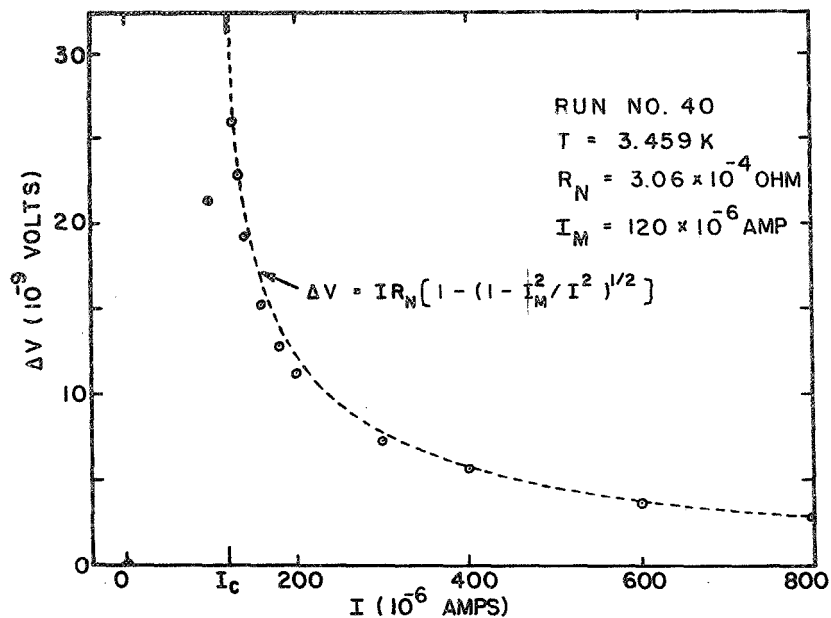


Fig.50 ΔV vs I , Run # 40.

In the same figure, Eq.IV.D.3 has been plotted for $I_m = 120 \times 10^{-6}$ amps and $R_N = 3.06 \times 10^{-4}$ ohms. The agreement is good.

IV.F. The Modification of the I-V Characteristics With a Control Current.

It was found that, with the addition of a second current into the contact, the I-V characteristics could be modified. The circuit description is in Sec.II.F.5. The current was introduced by means of the gold film, and it would flow from the film, through part of the junction (the actual flow pattern would be rather complicated and has not been analyzed) and into one of the tin wires. The current was considered positive if it flowed in the direction of the junction current.

The family of I-V characteristics obtained in this manner are somewhat similar in appearance to those of transistors. However, the mechanism is not presently understood and results found so far show a gain of less than 1 (current gain). No explanation for the effect will be attempted here. A typical family of curves, at a constant temperature of 1.36K, is shown in Fig.51.

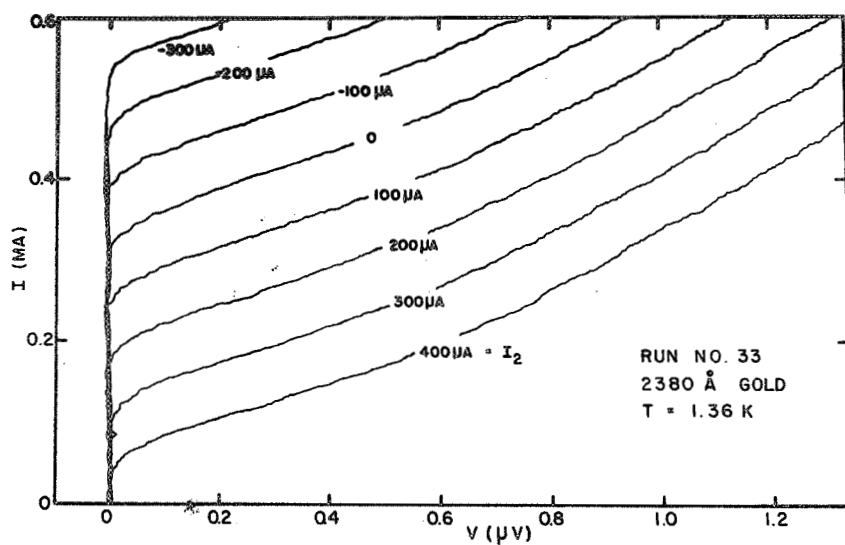


Fig.51 A Family of I-V
 Characteristics, for Run # 33, With a Second
 Current Introduced Into the Junction.

V. Conclusions.

Using a sensitive phase-lock technique, the SNS mechanical contact junction has been investigated and found to behave like an SIS Josephson junction. This supports the findings of Clarke²⁴, who made similar observations on thin film SNS junctions, with copper as the normal metal.

The current-voltage characteristics of the SNS junction have been found to obey the relation,

$$V = I_m R_N [1 - (I_m^2 / I^2)]^{\frac{1}{2}}$$

predicted by Stewart³⁸. The effects of fluctuations upon the I-V characteristics, predicted by Ambegoakar and Halperin⁴⁰, have also been observed, and correspond to a noise temperature of about 80K.

A technique was developed to determine the magnetic properties of the Josephson junction from its voltage-magnetic field characteristics. The observed oscillations, ΔH , of V with H , were used to determine the current bearing area of the contact. This was found to be approximately the same as the load bearing area ($\sim 10^{-5} \text{ cm}^2$)

in contradiction with earlier results⁴³. The load bearing area was observed microscopically, visually confirming the calculated area. In addition, an expression for ΔV vs H was derived for the case when $I > I_m$.

$$\Delta V = IR_N [1 - (1 - I_m^2/I^2)^{\frac{1}{2}}]$$

This result was verified by experiment, and provides additional confirmation for the presence of excess supercurrents³⁸ in the junction.

The resistance-temperature characteristics of the junction, illustrative of the transition from the normal state to the superconducting state, were plotted and their shape was qualitatively explained by the theory of fluctuations and excess supercurrents.

It was found that a second current, introduced directly into the normal metal area of the junction, can change the I-V characteristics and act as a control current. The gain (if this effect were used for amplification) is currently a fraction of unity, and a theory for the effect has not been attempted.

The critical current density of the junction was

found to be dependent on self-fields near T_c . The dependence is a function of temperature and the effect must be compensated by externally applied fields in order to obtain completely valid data.

The simple model of a SNS junction, proposed by deGennes¹⁹ and used by Clarke²⁴ to describe the thin film SNS junction, was not adequate to describe the current density of the mechanical contact junction. A modification of this theory has been made to account for the higher resistance of this type of junction. An expression for the current density was found to be,

$$\ln j_c = a_1 - \delta_{EP} / \xi_{EP} - \pi r^2 R_N / e_m \xi_m$$

where ξ_{EP} is the coherence length in the gold, δ_{EP} is the thickness of the gold (electroplated), e_m is the resistivity of a boundary layer assumed to be responsible for the contact resistance R_N , ξ_m is the coherence length in this boundary layer, the contact area is πr^2 and a_1 is a constant. With this model, the current density was reasonably well accounted for and the data yielded a value of $\xi_{EP} = 890 \text{ \AA} @ 2K$ and $e_m \xi_m = 7.4 \times 10^{-9} \text{ ohm-cm}^2 @ 2K$.

This model also predicts a temperature dependence for the critical current density,

$$\ln j_c(t) = C'_0 + f(t) - C'_I t^{\frac{1}{2}}$$

where C'_0 and C'_I are temperature independent constants. $f(t)$ has a known temperature dependence and has been plotted (see Fig.4). C'_I can be calculated from measured parameters and the predicted slope of $\ln j_c - f(t)$ vs $t^{\frac{1}{2}}$ gives reasonable agreement with the data.

With the addition of another layer of gold (N) to the junction, the current density is found, from the model, to be,

$$\ln j_c = a_1 - \delta_{EP} / \xi_{EP} - \delta_N / \xi_N - \pi r^2 R_N / e_m \xi_m$$

The experimental results fit this expression with reasonable agreement.

It had been hoped that the clean limit of the gold would be reached by growing the additional N layer as a single crystal. From the temperature dependence of the critical current density, it appears that this goal was not obtained.

BIBLIOGRAPHY

1. H. Kamerlingh Onnes, Leiden Comm., 122b, 124c (1911).
2. H. Kamerlingh Onnes, Leiden Comm., Suppl.No.34 (1913).
3. W. Meissner and R. Ochsenfeld, Naturwiss 21, 787 (1933).
4. C. Gorter and H.B.G. Casimir, Physica 1, 306 (1934).
5. P.G. deGennes, Superconductivity of Metals and Alloys (W.A. Benjamin, Inc., New York, 1966) Chapter 1.
6. F. London and H. London, Proc. Roy. Soc. A149, 71 (1935).
7. F. London and H. London, Physica 2, 341 (1935).
8. A.B. Pippard, Proc. Roy. Soc. (London) A203, 210 (1950).
9. A.B. Pippard, Proc. Roy. Soc. (London) A216, 547 (1953).
10. H. Frölich, Phys. Rev. 79, 845, (1950).
11. L.N. Cooper, Phys. Rev. 104, 1189, (1956).
12. J. Bardeen, L.N. Cooper and J.R. Schrieffer, Phys. Rev. 106, 162, (1957); 108, 1175 (1957).
13. V.L. Ginzburg and L.D. Landau, J.E.T.P. 20, 1064 (1950).
14. Superconductivity (Marcel Dekker, Inc., New York, (1969) edited by R.D. Parks, Chapters 8, 1, 6 and 9.
15. E.A. Lynton, Superconductivity (John Wiley & Sons, New York, (1964).
16. deGennes, see ref. 5, p. 178.
17. deGennes, see ref. 5, p. 225.
18. deGennes, see ref. 5, p. 233.
19. P.G. deGennes, Rev. Mod. Phys. 36, 224, (1964).
20. L.P. Gor'kov, J.E.T.P. 36, 1918 ; 37, 833, 1407; Soviet Physics JETP 9, 1364 (1959).
21. L.P. Gor'kov, J.E.T.P. 34, 735; Soviet Physics JETP 7, 505 (1958).
22. L.P. Gor'kov, Soviet Physics JETP 10, 593, 998 (1960).
23. G. Deutscher and P.G. deGennes, see ref. 14, p. 1006.
24. J. Clarke, Proc. Roy. Soc. A308, 447 (1969).
25. N.R. Werthamer, Phys. Rev. 132, 2440 (1963).
26. H. Meissner, Phys. Rev. 109, 686 (1958).
27. B.D. Josephson, Phys. Letters 1, 251 (1962).

Bibliography Cont'd

28. P.W. Anderson, Rev. Mod. Phys. 38, 298 (1966).
29. G. Rickayzen, see ref. 14, p.75.
30. P.W. Anderson and J.M. Rowell, Phys. Rev. Let. 10, 230 (1963).
31. B.D. Josephson, Rev. Mod. Phys. 36, 216 (1964).
32. J.M. Rowell, Phys. Rev. Let. 11, 200 (1963).
33. R.P. Feynman, R.B. Leighton and M. Sands, Lectures on Physics (Addison-Wesley, Mass. 1964) Vol. III, Ch. 21.
34. R.C. Jaklevic, J.J. Lambe and A.H. Silver, Phys. Rev. Let. 12, 159 (1964).
35. R.A. Ferrell and R.E. Prange, Phys. Rev. Let. 10, 479 (1963).
36. Feynman et. al., see ref. 33, Vol. II, p. 15-10.
37. J. Bardeen and J.R. Schrieffer, Progress in Low Temperature Physics III (1961), p.70.
38. W.C. Stewart, Applied Physics Letters 12, 277 (1968).
39. Y.M. Ivanchenko and L.A. Zil'berman, Exp. i. Teor. Fiz. 55, 2395 (1968).
40. V. Ambegaokar and B.I. Halperin, Phys. Rev. Let. 22, 1364, (1969).
41. S. Shapiro, Phys. Rev. Let. 11, 80 (1963).
42. J.E. Zimmerman and A.H. Silver, Phys. Rev. 141, 367 (1966).
43. H. Meissner, Studies of Contacts With Barriers in Between, ONR Report Nonr. 248 (49), (1959).
44. A.V. Bassewitz and G. v. Minnigerode, Z. Physik 181, 368 (1964).
45. National Bureau of Standards Monograph 10 (June 1960).
46. J.W. Matthews and E. Grumbaum, Phil. Mag. 11, 1233 (1965).
47. P. Tholfsen, Ph.D. thesis, Stevens Institute of Technology, unpublished (1969).
48. W.F. Koehler, Jour. Opt. Soc. Amer. 43, 739 (1953).
49. R.F. Duffy, Ph.D. thesis, Stevens Institute of Technology, unpublished (1964).

Bibliography Cont'd.

50. K. Fuchs, Proc. Camb. Phil. Soc. 34, 100 (1938).
51. R.B. Dingle, Proc. Roy. Soc. London A201, 545 (1950).
52. E.H. Sondheimer, Advan. in Physics 1, 8 (1952).
53. Handbook of Physics and Chemistry, 36 (1954-55).
54. McDonald, Encyl. Phys., XIV (Springer-Berlin, 1956)
p.188.
55. R. Holm, Electric Contacts (Hugo Gebers Forlag,
Stockholm, 1946), p. 16.
56. Nils L. Muench, Phys. Rev. 99, 1814 (1955).
57. E.A. Lynton, see ref. 15, p. 25.

ACKNOWLEDGEMENTS

I would like to thank Professor Hans Meissner for the inspiration and guidance given me during the course of this work. I must also express my appreciation to Mr. Gunther Wirth for his fine machine work and his optimistic outlook. I am grateful to Mr. George Prans for his assistance with some of the helium runs, and, also to Mr. James Walsh for building some of the electrical equipment. I would like to thank the National Aeronautics and Space Administration for its contract support, and the National Science Foundation for a Traineeship for a part of this work. I should also like to thank the Stevens Physics Department for the award of an assistantship and the use of its facilities. Finally, I would like to express my deepest thanks to my wife, Ellen, for her assistance and her constant encouragement.